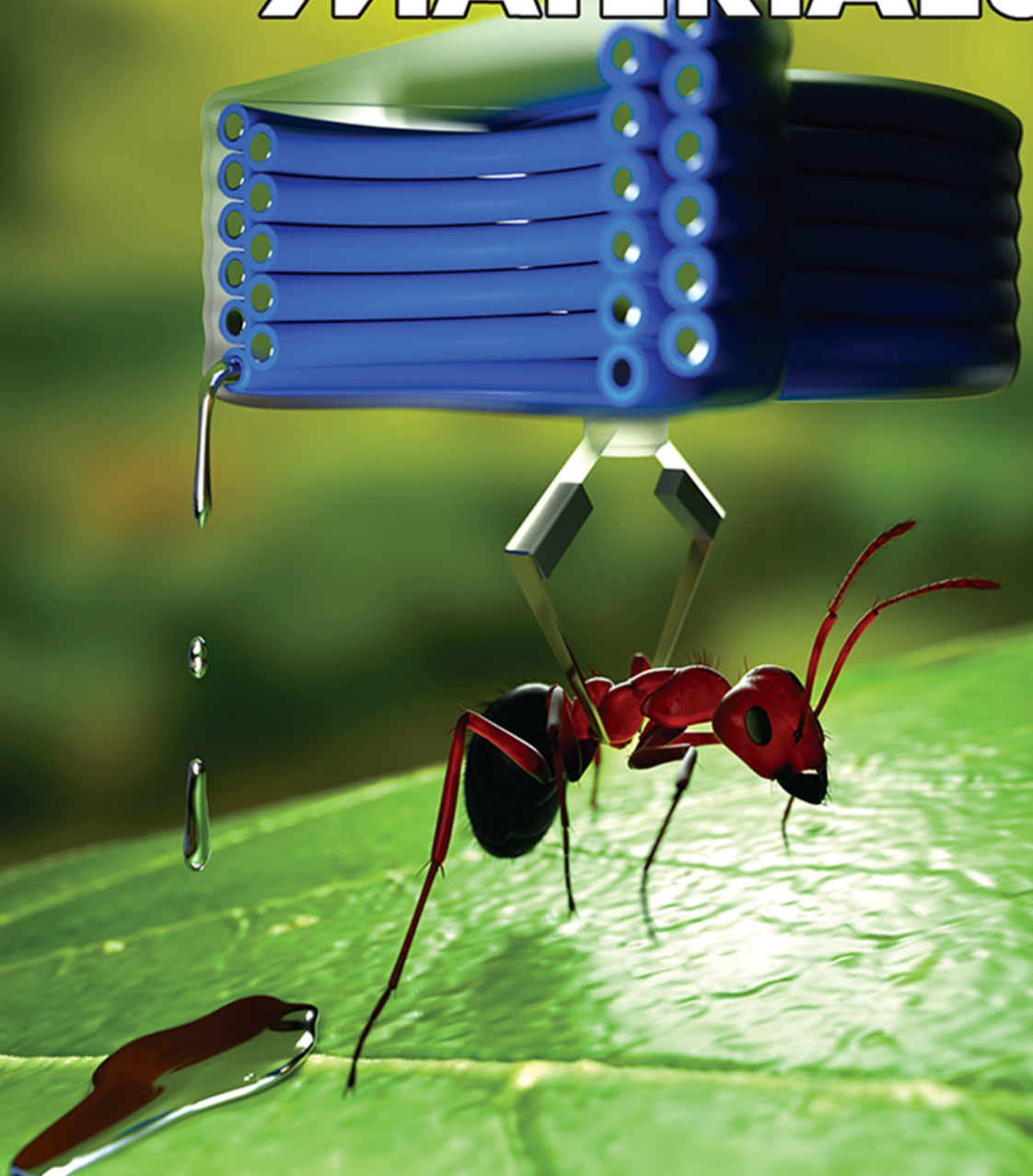


Vol. 28 • No. 18 • May 4 • 2018

www.afm-journal.de

ADVANCED FUNCTIONAL MATERIALS



WILEY-VCH

Miniature Soft Electromagnetic Actuators for Robotic Applications

Thanh Nho Do, Hung Phan, Thuc-Quyen Nguyen, and Yon Visell*

Electromagnetic actuators (EMAs) serve the majority of motion control needs in fields ranging from industrial robotics to automotive systems and biomedical devices, due to their unmatched combination of speed, precision, force, and scalability. This paper describes the design and fabrication of miniature soft EMAs that operate based on the Lorentz force principle. The actuators are fabricated from silicone polymer, liquid metal (LM) alloy (eutectic gallium indium, EGaIn), and magnetic (NdFeB) powder. They are small, intrinsically deformable, and can be fabricated using simple techniques. The central elements of the actuators are fine, 3D helical coil conductors, which are used as electromagnetic inductors. The coils are formed from stretchable filaments that are filled with a LM alloy. To achieve high power densities, the filaments themselves may be fabricated from colloids of EGaIn microdroplets in a silicone polymer matrix, allowing them to dissipate heat and accommodate high currents, and thus high forces. Millimeter-scale cylindrical actuators are demonstrated for linear high frequency motion and articulated devices for bending motion. These actuators are applied in a vibrotactile feedback display and in a miniature soft robotic gripper.

1. Introduction

Soft robotic systems are of increasing interest due to the promise they hold for ensuring safe human–robot interaction and highly robust and adaptable operation in complex, unstructured environments.^[1–9] They offer many advantages over conventional systems made of rigid elements. They can flexibly adapt to a great variety of configurations, and to different mechanical settings, can ensure safe cooperation with humans, and can facilitate the coordination of large numbers of degrees of freedom.^[8] Many types of stretchable and wearable sensors, soft actuators, soft energy harvesters, and storage devices have been developed,^[10–13] often motivated by applications

in robotics, healthcare, and other domains. Mechanical systems based on soft actuators are also adaptable to systems of greatly varying length scales, ranging from miniature grippers, to mobile robots, wearable tactile displays, and biomedical devices.^[5,8,14] Methods of actuation for soft robotics include tendon-driven actuation, smart materials, such as shape memory polymers (SMPs), shape memory alloys (SMAs), pneumatic fiber braids, pneumatic polymers elastomers, hydrogels or electroactive polymers (EAPs).^[5,8,9,15] Despite their promise, all of these methods possess limitations in performance and controllability in comparison to systems based on electromagnetic motors. SMAs and SMPs can achieve large strains when heated, but are limited by heating, cooling, and hysteresis effects. Pneumatic polymers require external air power, respond at speeds that are limited by

the supply pressure, and are difficult to control proportionally. Soft EAPs comprise two main categories: ionic and electric. Ionic EAPs are usually limited by their poor coupling efficiencies and relatively slow actuation speeds. Electric EAPs require high voltages (typically 100 V to several kV),^[5,16] which can pose design problems and, in some cases, safety issues.^[17] In addition, they typically produce weak force and careful design is needed to avoid mechanical instabilities.

Electromagnetic actuators (EMAs) can be readily designed and driven with large bandwidths, especially when compared with devices that operate as capacitive loads (such as electrostatic actuators). The use of high performance magnetic actuators, such as the ones in magnetically driven robots, has attracted growing attention.^[18–24] In one form, these actuators are operated via the control of magnetic microparticles in a polymer matrix using an external magnetic field from an electromagnet. By varying the orientation and magnitude of such a field, the deformable magnetic composite may be controlled in torque, deformation, elongation, contraction, or bending.^[5] These actuated structures can achieve fast response times, high dynamic ranges, small size, high power efficiency, and low driving voltages (typically 0 to 30 V).^[5,9,25] As a result, they have been successfully utilized for creating a variety of high performance mechatronic and microrobotic systems, including swimmers, crawling devices, micropumps, and many others.^[5,9]

There are several challenges that have prevented the development of high performance EMAs for soft robotics.

Dr. T. N. Do, Prof. Y. Visell
 Department of Electrical Computer Engineering
 Media Arts and Technology Program
 California NanoSystems Institute
 University of California
 Santa Barbara, CA 93106, USA
 E-mail: yonvisell@ece.ucsb.edu
 Dr. H. Phan, Prof. T.-Q. Nguyen
 Department of Chemistry and Biochemistry
 University of California
 Santa Barbara, CA 93106, USA

 The ORCID identification number(s) for the author(s) of this article can be found under <https://doi.org/10.1002/adfm.201800244>.

DOI: 10.1002/adfm.201800244

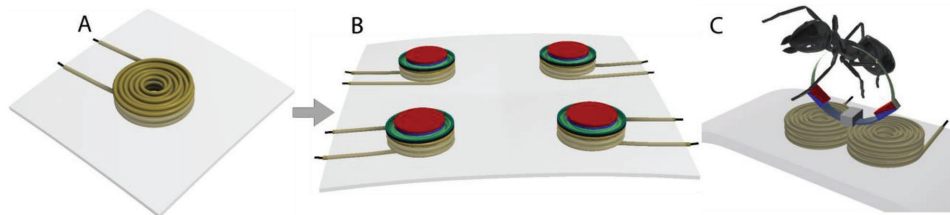


Figure 1. Soft electromagnetic actuators for wearable tactile display and miniature robotics applications. A) Soft 3D helical coil adhered onto a soft silicone layer. B) An array of soft vibrotactile actuators, formed via the coupling of soft inductors with permanent magnets and flexible membrane suspensions; see Section 2. C) A miniature soft magnetic gripper, suited to micromanipulation tasks, formed from soft 3D helical coils and magnetic arms, shown with an ant.

Conventionally, such devices use rigid conductive wire inductors, such as copper wire coils, to generate time-varying magnetic fields via applied currents, and to exert forces on permanent magnet components. While wire electromagnetic inductors may be introduced into soft materials,^[26–28] their rigidity can greatly limit deformability, and can reduce the durability and longevity of the materials due to stress concentrations that develop at material boundaries. Among soft conductive materials, liquid metals (LMs) including eutectic alloys Galinstan (68% Ga, 21.5% In, and 10% Ti) and gallium indium (EGaIn, 75% Ga, 25% In by mass) have attracted considerable attention for applications in stretchable electronics and soft robotics. These materials have excellent electrical conductivity (EGaIn, $\sigma = 3.4 \times 10^4 \text{ S cm}^{-1}$) and thermal conductivity (EGaIn, $\kappa_e = 24.9 \text{ W m}^{-1} \text{ K}^{-1}$), low melting point (EGaIn, 15.7 °C), low vapor pressure, and low toxicity.^[29–31] When introduced into channels of a soft substrate, such as a polymer elastomer, they can facilitate a wide range of applications from soft wearable sensors, to soft electronic interconnects, stretchable RF antennas, and soft liquid metal actuators.^[10,30–32]

Several microfluidic and soft lithography methods have been developed for the creation of simple planar devices based on liquid conductors and elastomers,^[30,31,33,34] but the fabrication of 3D structures, which are needed in order to realize most functional actuators, is challenging using standard methods. In one such method, multiple layers of soft materials (e.g., polydimethylsiloxane (PDMS), or soft silicone polymers) are patterned and sealed together to form an internal 3D channel.^[12,35–38] In another, sacrificial and 3D printed molding methods, using solvent casting, are used, but these methods require harsh chemical processing, and do not scale to small sizes.^[39,40] The fabrication of stretchable radio frequency (RF) antennas and inductors for stretchable acoustic devices has been previously reported,^[33,41] but this work has often been limited to planar (2D) structures, or to very simple multilayer topologies that are not well suited to actuator design.^[42–44] Recently proposed methods for 2D composite fabrication with eutectic alloys can yield novel functionalities, including semiconducting devices,^[45] but are not amenable to the realization of actuators.

Here we propose new methods for the design and fabrication of soft, composite structures for miniature EMAs suited to applications in areas ranging from tactile displays to medical robots. We present a simple fabrication process based on a roller coating and stencil printing method, which allows us to realize highly conductive, stretchable filaments that we use to create inductors, such as helical coils, with a wide variety of

possible geometries. This method is simple and effective and is amenable to integration in composite devices and circuits, and to fabrication in research lab settings or to being adapted for manufacturing.

The deformability of these actuators holds promise for many applications. Their ability to conform to the human body or other structures is advantageous for wearable computing and for soft surgical robots that work in complex and unstructured environments. To demonstrate advantages of the proposed methods, we design and fabricate soft electromagnetic vibrotactile actuators (EMVAs) and a soft, articulated miniature robotic gripper that manipulated various objects or loads (Figure 1). These devices are made from 3D helical coils, LM alloy, soft silicone substrates, permanent magnets, and magnetic microparticles. They are soft, inexpensive, and able to realize vibration or motion for wearable computing and robotics applications. We introduce theoretical models for the devices and validate them in experiments.

2. Development of a Soft 3D Electromagnetic Inductor

2.1. Fabrication of Soft 3D Helical Coil with Stretchable Conductive Channels

We developed a new process (Figure 2) for the design and fabrication of 3D helical coils for use in soft electronics. First, a liquid elastomer emulsion with high thermal conductivity (Section 2.2) is deposited in a thin layer (around 150 µm) on a flat surface using a stainless steel roller (Figure 2A). A fine carbon fiber rod (200 µm) is slowly rolled onto the thin silicone composite, followed by heating with a hot plate (Figure 2B,C). The cured silicone layer is peeled from the rod to form a hollow elastomer filament. The wall thickness of the hollow filament is ~120 µm (see Figure S5, Supporting Information for more details). LM alloy is injected into the hollow fiber using a fine needle and syringe to form a long, stretchable, conductive hollow filament (Figure 2D). Wire electrodes are inserted into the ends, forming electrical connections, and the hollow filaments are then sealed. The soft hollow filament is wrapped around a plastic cylinder to form a 3D helical coil (Figure 2E), and, to maintain its shape, is integrated with a soft silicone substrate (Figure 2F). To form actuators, the coils can be mechanically coupled to permanent magnets and flexible elastic membranes.

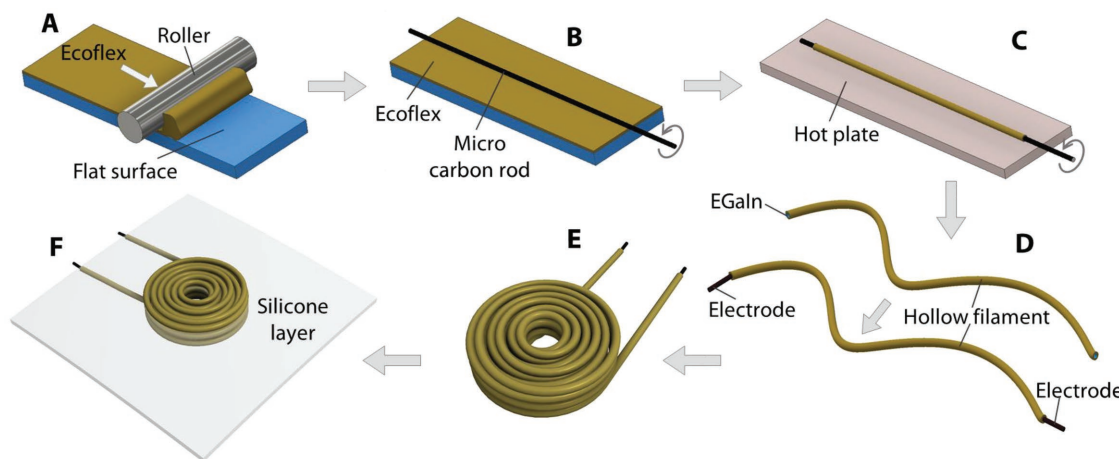


Figure 2. Fabrication process for the soft, 3D helical coil inductor. A) A thin layer of liquid silicone elastomer (Ecoflex 0030) is laminated onto a flat surface using a stainless steel roller. B) A fine, carbon fiber rod is rolled onto the thin silicone layer. C) The laminated layer and rod are heated via hot plate. D) Liquid metal alloy (EGaIn) is injected into the hollow filament, and electrodes are inserted into the two ends. E) The hollow filament is wound to form a 3D helical coil. F) 3D helical coil is adhered to a soft silicone layer.

In the operation of actuators made from these coils, a magnetic field B_c is generated by the coil when a current is applied, as can be calculated from first principles. Here, we modeled the magnetic field for the 3D helical coil as a solenoid inductor. The cross section is shown in Figure S1 of the Supporting Information. We apply Ampere's law to calculate the magnetic field strength at a point P located at distance z from the coil center on the axial z -axis (see Equations (S1)–(S3), Supporting Information). The amount of electrical power dissipated via Joule heating can also be calculated directly from the electrical resistance of the coil (see Equations (S4) and (S5), Supporting Information).

From the resulting equations, the magnetic field generated by the coil depends on an array of factors, including the number of turns, size of coils, current applied, permeability, and distance between the coil center and the object. In addition, the power consumption and thermal behavior also depend on the current, resistance, material properties, and ambient temperature. For a given coil geometry, the field strength (and hence force) and power consumption are constrained by heating, which, for fixed current, depends on resistance of the conductor and the thermal conductivity of the filament sheath.

2.2. Elastomer Filaments Inductors with High Thermal Conductivity

To achieve high power densities and field strength, EMAs must typically be driven with large currents (>1 A). For soft polymer devices like those presented here, this can readily lead to thermal failure, due to the inefficient thermal transport of elastomers, and becomes a limiting factor. One method for reducing heating is to enhance the electrical conductivity of the liquid metal by suspending conductive (silver or gold) nanoparticles in it using one of several previous described techniques.^[46–51] The resulting solutions are invariably high in viscosity, making them difficult to introduce into solid substrates. As an alternative, we engineered thermally efficient

inductors using elastomer filaments formed from colloids of LM alloy in a polymer matrix, yielding greatly increased thermal transport and thus increase the current and force limitations.^[29,52] Thermal transport in soft elastomers is limited by the dynamics of elastic vibrations, or phonon transport properties.^[29,52–54] From kinetic theory one finds that thermal conductivity κ_e is given by $\kappa_e \approx v C_V \lambda / 3 = (E/\rho)^{1/2} C_V \lambda / 3$, where v is the speed of sound, E is the elastic modulus, ρ is the density, C_V is the volumetric specific heat, and λ is the mean free path of phonons.^[55] Thus, low modulus dielectric materials typically exhibit low heat transfer. Various methods for overcoming this limitation on thermal transport in compliant materials have been proposed, often through the introduction of filler materials with higher thermal conductivity.^[53] Among these, a recently introduced family of engineered elastomer colloids with elongated inclusions of LM,^[29,52] which function as thermally conductive pathways, is especially attractive for its ability to preserve the low stiffness and high strain limit of the polymer, and to achieve high thermal conductivities, approaching $10 \text{ W m}^{-1} \text{ K}^{-1}$.

To apply this, we fabricated a composite elastomer via shear mixing of EGaIn with a liquid polymer elastomer (Ecoflex 0030) at specified weight ratios to produce an emulsion of elongated LM domains within the polymer medium, which, upon curing, yields an elastic colloid with improved thermal conductivity, as demonstrated below (see the Experimental Section for complete details).

We used this material to fabricate elastomer filaments with several different mass ratios of EGaIn, and from which we made 3D helical coils (Figure 2). The increased thermal conductivity allows the resulting coils to be operated at higher currents (and hence forces) for longer times without undergoing thermally induced mechanical failure or overheating (Figure 3).

We characterized the heating of coils formed from composite elastomers with different mass ratios of LM (0%, 30%, 60%, and 90%) using a thermal imaging camera (FLIR A35 Series, FLIR Systems, Inc., USA). Initially, the coils were

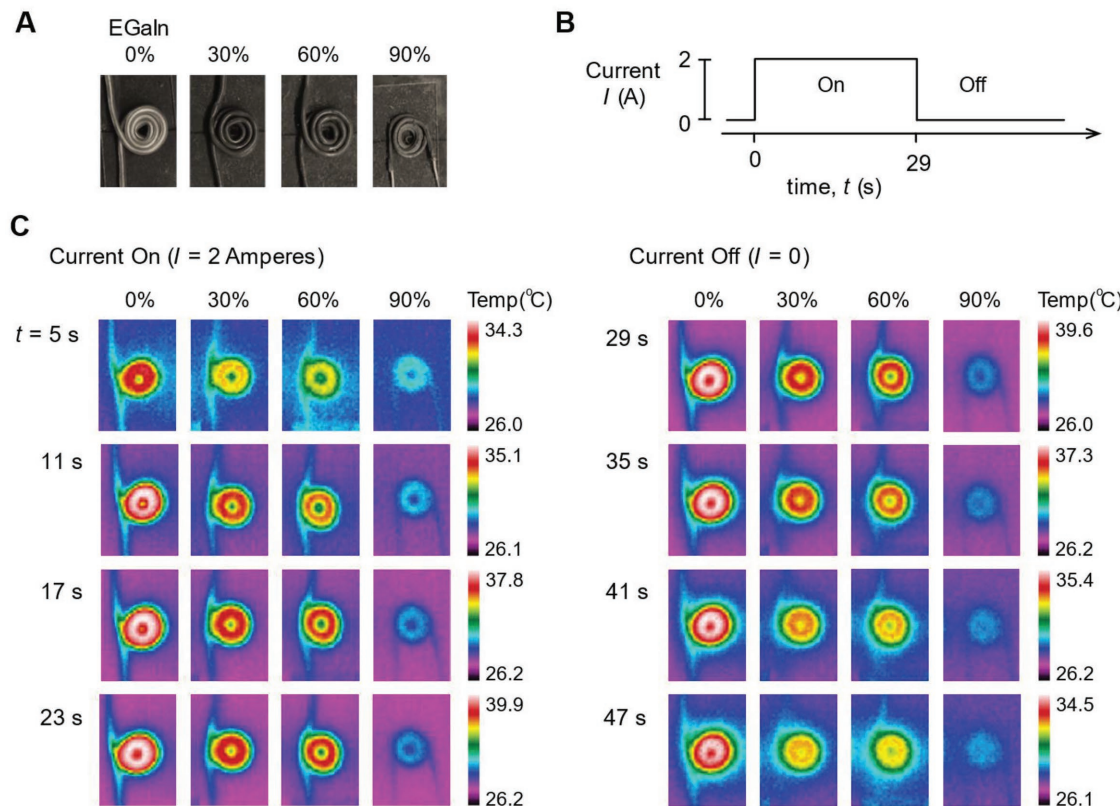


Figure 3. Enhanced thermal regulation through the use of colloids of silicone polymer with liquid metal alloy (EGaIn). A) Coil heating with different mass ratios of EGaIn and polymer: 0%, 30%, 60%, and 90%. B) A DC current of 2 A was switched on for 29 s, then switched off. C) As the EGaIn ratio increased, the surface temperature remained lower, and decreased more rapidly when the current was removed.

unpowered. Subsequently, a high current of 2 A was applied for 29 s, then removed (Figure 3B). The thermal imaging results indicate that the coils formed from composite elastomers with the highest mass ratios dissipated heat most efficiently, leading to far lower surface temperatures. At 90% mass ratio, the surface temperature remained below 30 °C, while the surface temperature of the sample with 0% mass ratio grew monotonically, reaching 40 °C. When the current was removed, the surface temperatures dropped more rapidly for the composite elastomer coils, indicating that these devices can achieve better thermal performance under both sustained and transient loading with high currents without degrading their mechanical performance.

3. Applications of Soft 3D Helical Coils

3.1. Soft Vibrotactile Actuators (SVAs)

Haptic technologies—electronic displays for the sense of touch—have received growing interest in the last few decades. Such displays, analogous to graphical display for vision, deliver mechanical stimuli to stimulate the skin. Among the many types of haptic devices, vibrotactile displays, based on the application of mechanical vibrations to the skin, are the most widespread and investigated because of the ease of designing and driving them.^[56] To date, vibrotactile display devices have

used rigid electromagnetic motors, piezoactuators, electroactive polymer actuators, or dielectric actuators, among others,^[57–60] all of which involve tradeoffs in rigidity, performance, or complexity. Although dielectric elastomer actuators have attracted attention in haptics, as soft devices that can respond quickly and that can be made compact, they typically require high voltages (often 1 kV or more), complex fabrication procedures, and carefully controlled mechanics; also, these devices involve tradeoffs between size, displacement ratio, and force that make it difficult to achieve adequate power densities.^[61]

The SVAs we introduce here can operate at low voltages and are facile to fabricate. They can be designed as individual elements or as arrays that are amenable to integration in skin-worn interfaces, as demonstrated in several prototypes presented here (Figure 4). As discussed in Section 2.2, coils may be fabricated from colloids of polymer with LM microdroplets where high thermal conductivity is required. In the illustrative demonstrations presented here, which required only low current values, and were thus not limited by thermal performance, we selected noncolloidal polymer as the substrate, thus simplifying the fabrication procedure and description.

To fabricate the SVAs (Figure S2, Supporting Information), first, the helical coil (Figure 2) is attached to a silicone substrate by adhering it with a layer of liquid uncured Ecoflex 0030 (Smooth-On, Inc, Easton, PA, USA). It is then cured at 60 °C for 1 h. Next, a silicone membrane (Ecoflex 0030) is bonded to the coil, and a permanent magnet is bonded to its opposite

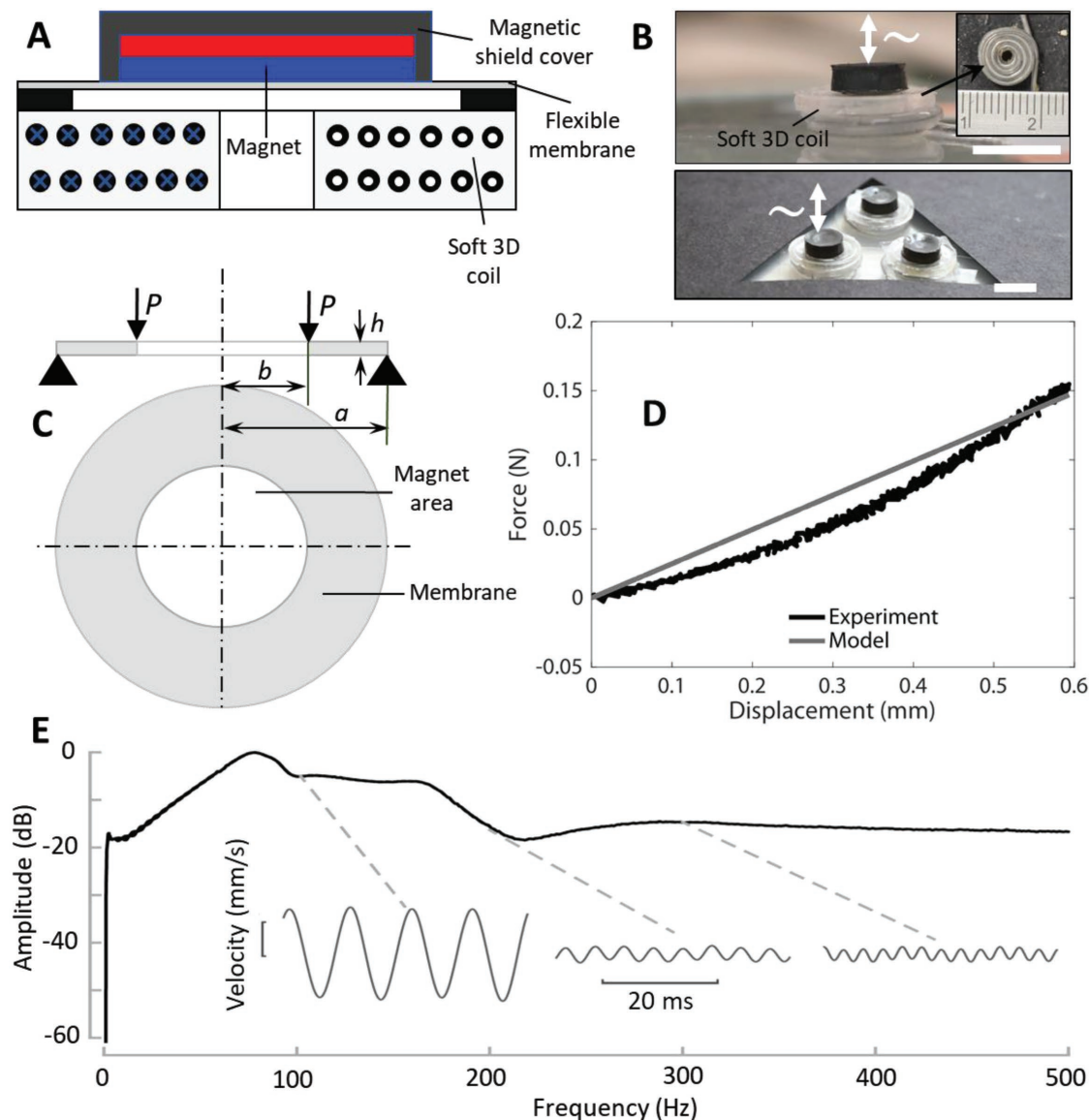


Figure 4. Soft electromagnetic vibrotactile actuators. A) Structure of a soft electromagnetic actuator. B) Fabricated soft electromagnetic vibrotactile actuators. C) Solid mechanical model, consisting of an annular plate subjected to a load at the radius b of the magnet. D) A comparison of model predictions and experimental measurements of the actuator displacement versus force deformation show close agreement. E) The useful actuator response extends beyond 500 Hz, overlapping virtually all of the range of sensitivity of tactile sensation. Parameters for fabricated device $b = 3$ mm, $a = 4$ mm, $h = 0.12$ mm, $E = 125$ KPa, $\vartheta = 0.5$. Scale bar: 5 mm.

face (Figure 4A). To create arrays of vibrotactile actuators (VAs), multiple 3D helical coils are attached and assembled on a single substrate. To avoid otherwise high interaction forces between neighboring magnets, we fabricated magnetic shield, consisting of a high magnetic permeability elastomer composite, covering all but the coil side of the magnet (Figure 4A; Figure S2, Supporting Information). This ensures that each vibrotactile actuator can respond independently, and that the static magnetic forces do not disturb the soft structures involved.^[62] The dynamics of the resulting actuators can be modeled by building on the results of Section S6 of the Supporting Information, and accounting for the motion of the magnet and membrane. The membrane deformation is modeled as

a simply supported annular plate with outer radius a , corresponding to the membrane, and inner radius b (Figure 4C), corresponding to the radius of the permanent magnet bonded to it.^[63] The maximum deflection δ_{\max} is at the inner edge of the membrane, $r = b$. Using $F = 2\pi bP$, for small displacements, the maximum deflection in response to applied force F can be obtained from solid mechanics consideration, yielding a linear relation $\delta_{\max} = F g(a, b \vartheta, D)$, where the proportionality constant g depends on the geometric and material parameters of the device (see Equation (S17), Supporting Information).

To validate the proposed design and approach, we used the parameters corresponding to the fabricated device. Predicted values and results of real-time experiments are shown in

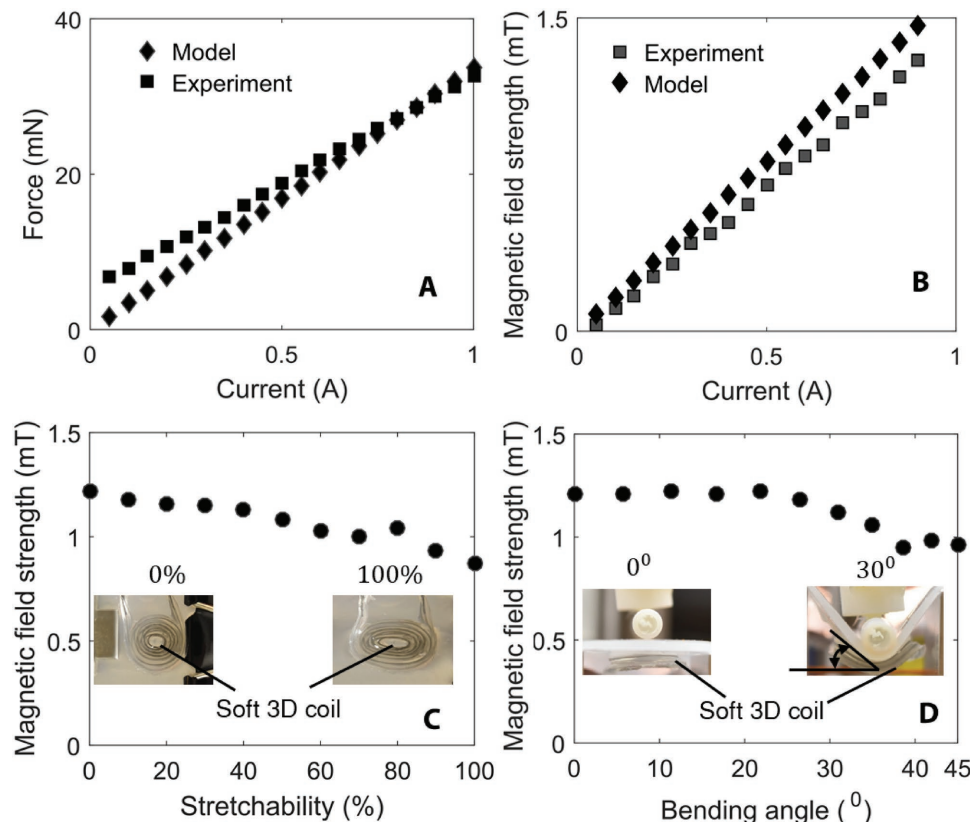


Figure 5. Soft 3D coil characterization. A) Magnetic force versus applied current: mathematical model and measurements. B) Magnetic field strength versus current: mathematical model and measurements. C) Magnetic field strength versus coil elongation. D) Magnetic field strength versus bending angle. The model parameters of the device are as $\mu_0 = 4\pi \times 10^{-7} \text{ JA}^{-2} \text{ m}^{-1}$, $N = 7$, $l = 3 \text{ mm}$, $R = 4.5 \text{ mm}$, and $z = (l/2 + 0.75) \text{ mm}$, $M_m = 1.48/\mu_0 \text{ Am}^{-1}$, $h_m = 4.15 \text{ mm}$, $R_m = 3.17 \text{ mm}$, where h_m and R_m are the height and radius of the permanent magnet, respectively.

Figure 4D. We applied forces that ranged from 0 to 0.15 N, measured the membrane displacement via a laser position sensor (Model IL-065, Keyence, USA). The displacement is approximately linear with the applied force ($F = K\delta_{\max}$, $K = 0.27 \text{ Nm m}^{-1}$). In implementations, this relation can be used to estimate forces between the magnet and the soft coil using sensed displacement information, which may be useful when other force sensing methods are not available. We also evaluated the actuator response to oscillating inputs. As shown in Figure 4E and Videos of the Supporting Information, the actuator readily responded to sinusoidal driving signals ranging from 0 to 500 Hz.

We also characterized the force F , which is described by Equation (S9) of the Supporting Information, generated by the soft coil to the external magnet with volume V_m and magnetization M_m . The results are reported in Figure 5A. A higher value of force can be achieved by increasing the number of turns N and the current I at the expense of greater power consumption. The magnetic force F of the coil on the external magnet for $I = 1 \text{ A}$ is $\approx 32 \text{ mN}$ corresponding to a displacement δ_{\max} of 0.23 mm. The work density of the VA is approximately $W_{\text{vibro}} = F\delta_{\max}/V_{\text{act}}$ or $W_{\text{vibro}} = 0.053 \text{ kJ m}^{-3}$ where $V_{\text{act}} = 1.531 \times 10^{-7} \text{ m}^3$ is the actuator volume. We also calculated the power consumption for the single VA (see Equation (S4), Supporting Information). With current $I = 1 \text{ A}$ and resistance $R_c = 0.9 \Omega$, the mean power consumption P_{vibro}

for a single actuator is 0.9 W. The energy conversion ratio η between the energy supplied to the actuator and the mechanical work is approximately $\eta = (F\delta_{\max})/(t_{\text{move}} P_{\text{vibro}})$ or 0.03% where $t_{\text{move}} \approx 0.03 \text{ s}$ is the travel time of the magnet from the origin to a position of 0.23 mm. A comparison of this device with other actuators is provided in Table S1 of the Supporting Information.

We also evaluated the magnetic field as a function of the applied current via a real-time experiment, using the design parameters given above, yielding close agreement, with some discrepancy at high currents (Figure 5B), likely attributable to the change in magnetic field with distance from the coil. We also evaluated the stretchability of these devices by under strain-controlled loading from 0% to 100% (step size 10%) and assessed their flexibility by controlling the bending angle of the supporting surface, from 0° to 45° (see Figure 5C,D). In both experiments, we applied a constant current ($I = 0.8 \text{ A}$) to the coil and measured the magnetic field immediately above the center of the coil (at $z = l/2$) using a Gauss meter (model 5180, F.W. Bell, USA). The nominal field strength of 1.2 mT decreased with bending due to the change in coil geometry (Figure 5C,D), reducing to a minimum of 0.85 mT for large values of strain and 0.9 mT for very large bending angles. Despite the modest flux loss, the devices remained functional throughout this range, and hold promise for applications in which stretchability and conformability are paramount. See also in Figure S7

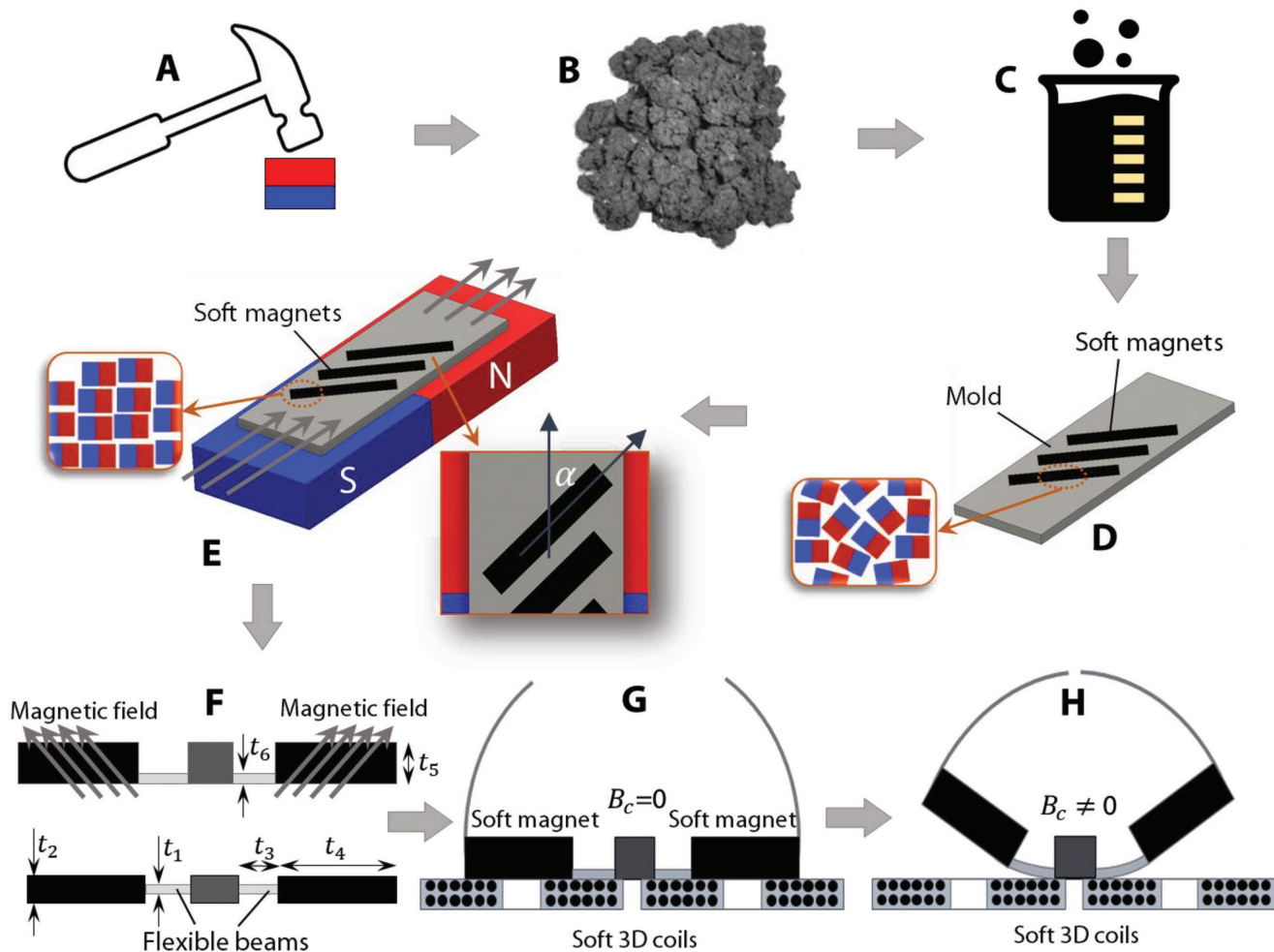


Figure 6. The fabrication process and working principle of the miniature soft electromagnetic gripper: A) Crush a permanent magnet (type N52) into B) microparticles, which are then C) mixed with liquid silicone polymer using a mixing machine. D) Pour the suspension of magnetic particles and polymer into a 3D printed mold. E) Align the mold above a permanent magnet to elicit a specified magnetization orientation. F) Side view and top view of the finished device where the magnetic arms are then mounted on a flexible beam. G) Soft gripper in the absence of magnetic field generated by the soft 3D coils. H) Soft gripper under the presence of applied magnetic field generated by the soft 3D coils.

and Videos of the Supporting Information for more details. To further evaluate the stretchability of the coil, we measured the change in resistance under the applied strain ranging from 0% to 100%. The results reveal a change in resistance with minimal effect on device performances (see Figure S5, Supporting Information). During the experiments, we held the current $I \leq 1$ A. Higher currents can be sustained if the coil is fabricated from the proposed thermal composite, as shown in Section 2.2.

3.2. Miniature Soft Electromagnetic Gripper (SEMG)

Advances in soft microrobotics may enable many applications, especially in healthcare industry, but the required technologies, and methods for fabricating them, are still developing. Here, we present a miniature soft SEMG that can flexibly grasp, hold, and release a specified object or tissue. The gripper is fabricated with the newly developed soft 3D helical coil (Section 2) and

soft magnets, which are briefly described here (see Figure 6). First, a permanent magnet (NdFeB, grade N52, K&J Magnetics, USA) is broken down into small magnetic particles using a hammer or planetary ball milling machine. Second, a liquid silicone (recommended by ratio 1:10 between the curing agent and elastomer, Sylgard 184 Silicone Elastomer, Dow Corning, USA) is homogeneously mixed with the magnetic powder at a weight ratio of 1:9. After mixing, the solution is poured into a 3D printed mold, and aligned with an external permanent magnet. The orientation of the magnetic polarization of the arms of the gripper ($\alpha = 25^\circ$) is specified by curing in an external magnetic field imposed by a high strength permanent magnet (Figure 6D,E). Curing is performed in an oven at 60 °C for 3 h. The magnetic arms are then mounted on a flexible beam (Ecoflex 0030, Smooth-On, Inc, Easton, PA, USA) (Figure 6F). After curing, the assembly is coupled to a pair of soft 3D helical coils, and the assembly is sealed via uncured Ecoflex 0030. Upon excitation of the coils, the arms of gripper may be independently controlled, opened, and closed by

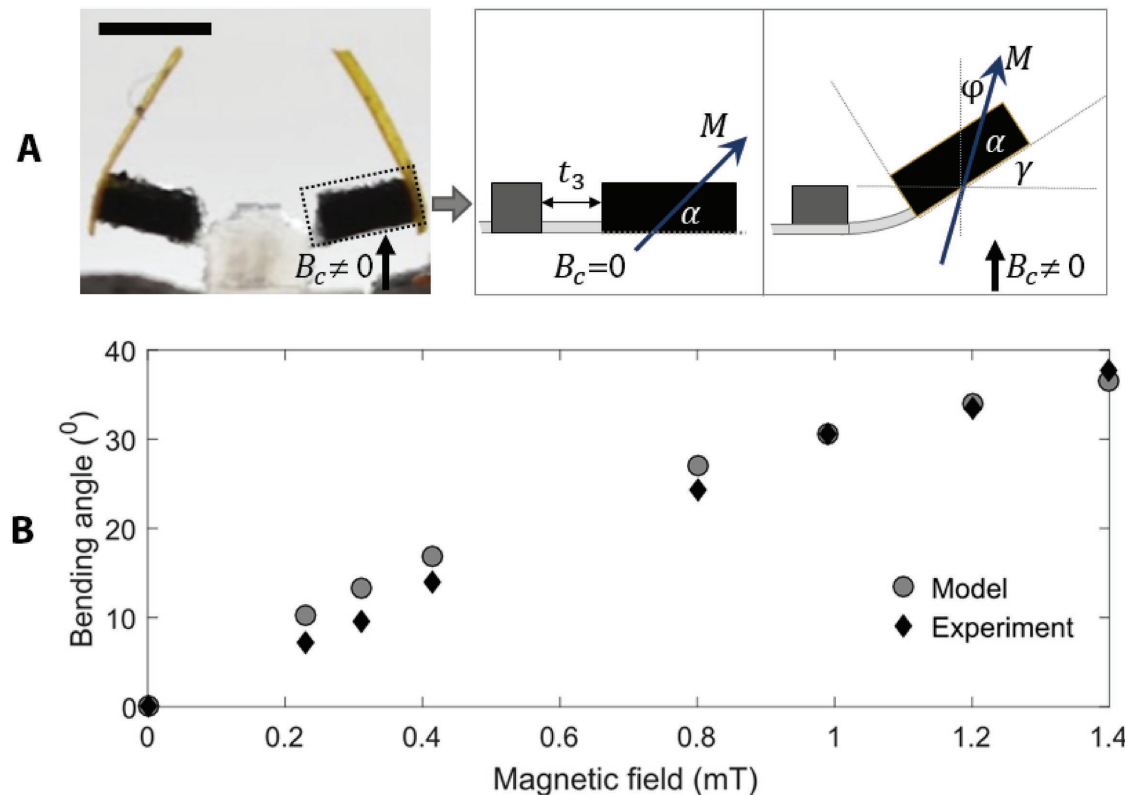


Figure 7. Validation experiments for miniature soft magnetic gripper. A) Schematic of bending angle γ for a single arm with attached soft magnets. B) Real-time measurement of applied magnetic fields versus bending angles for a single arm. The device parameters are $t_1 = 0.9$ mm, $t_2 = 1$ mm, $t_3 = 0.6$ mm, $t_4 = 1.9$ mm, $t_5 = 0.7$ mm, $t_6 = 0.23$ mm, $E = 125$ kPa, $\alpha = 25^\circ$. The magnetization value $M = B_r/\mu_0 = 137$ kAm $^{-1}$ (see Figure S3 and Equation (S22), Supporting Information). Scale bar: 2 mm.

magnetic fields produced by supplying current to the coils (Figure 6G,H).

To control the orientation or bending angle γ of the soft magnet of each arm, a magnetic field of magnitude B_c is imposed by applying the requisite current I to the soft 3D coil. We evaluated the resulting expression numerically and compared the predictions with the parameters that matched our gripper. The results are shown in Figure 7B and illustrate good agreement between the experiment and the model (Equation (S20), Supporting Information), for angles up to 40°.

To illustrate the utility of the SEMG, we demonstrate its ability to pick up a small foam, a PDMS cube, and a preserved carpenter ant (*Camponotus* sp., Figure 8). The weights for soft foam, ant, and PDMS cube are 2.89, 3.61, and 13 mg, respectively. In addition, the distance between the two tips of the opened and closed gripper is ≈3.88 mm and all objects are ≈2 mm wide (see Figure S6, Supporting Information). The soft gripper descends to the target object, and current is supplied to the coils, closing the grips.

The strength of the magnetic field, and force, depend on the driving current. Using the thermally efficient polymer filaments (Section 2.2) facilitated the use of higher currents and forces. The current is switched on, reversed, or switched off in the experiment to open and close the grip. In the validation, we used 14 turns of 3D soft coil in order

to generate a high magnetic field to the soft gripper. The amount of electrical power dissipated via Joule heating P_{grip} of a coil is around 1.296 W, corresponding to an applied current of 1.2 A. The work density ($W_{\text{grip}} = T\gamma/V_{\text{act}}$) or 0.25 Jm $^{-3}$. The energy conversion ratio between the power supply and the mechanical work ($T\gamma)/(t_{\text{move}}P_{\text{grip}})$ or 0.0049% where the torque $T \approx 0.18$ μ N m is estimated from Equation (S18) of the Supporting Information, $\gamma = 38^\circ$, and $t_{\text{move}} \approx 0.024$ s. The soft gripper is intrinsically fast, operating at time scales of tens of milliseconds, corresponding to a frequency bandwidth of 100 Hz or more. Comparison between the proposed soft gripper and others is presented in Table S1 of the Supporting Information. Further details are shown in Videos of the Supporting Information.

4. Conclusion

We developed and fabricated SEMAs, which are actuated based on the Lorentz force principle, via electrical current. The central innovation of our devices is a soft electromagnetic inductor made from 3D helical coils formed from fine, stretchable hollow filaments that are filled with a LM alloy conductor. By fabricating these filaments from a colloid of silicone polymer and EGaIn microdroplets, we enable them to achieve high thermal conductivity, facilitating greatly increased current handling,

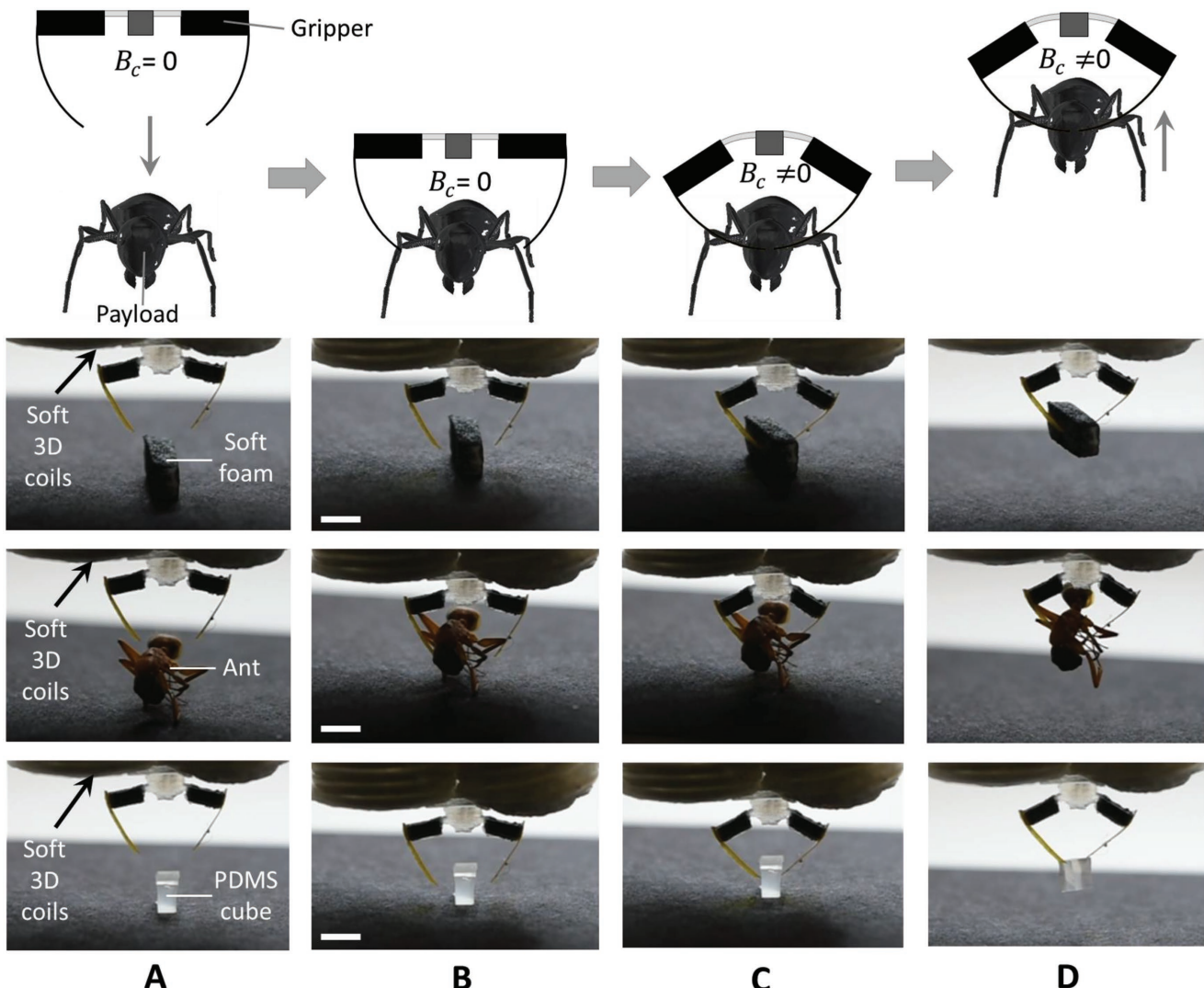


Figure 8. Manipulation process steps and experimental validation for the miniature gripper with a soft foam cube, an ant, and a PDMS cube. A) Initial position of the gripper. B) The gripper approaches vertically from the top to the payload. C) The gripper holds and lifts the payload. D) The gripper moves back to its original position. The objects are ≈ 2 mm wide. Videos for real-time experiments are presented in the Supporting Information. Scale bar: 2 mm.

and commensurately higher magnetic fields, and forces. Using these technologies, we demonstrate small scale cylindrical actuators capable of linear high-frequency motion. The performance of these devices exhibits close quantitative agreement with predictions of a mathematical model based on the Lorentz force principle. They prove capable of operating over a scalable range of voltages or currents, here ranging from 50 mA to >1 A, or 50 mV to 1 V, yielding displacements of up to 1 mm, and retained most of their performance when stretched up to 100%, or bent to angles of 38°. We apply these actuators in multipoint arrays, which are suited to providing tactile feedback in wearable devices, even as they stretch to conform to the skin. We also demonstrate multi degree-of-freedom devices that are capable of articulated motion and demonstrate their application in a unique miniature soft robotic gripper, which proved capable of manipulating (grasping, lifting, and releasing) miniature loads.

The proposed SEMAs have several key advantages: (i) They are fast, capable of operating at high frequencies. (ii) They can operate at low voltages. (iii) They are thermally efficient, enabling them to achieve high transient or sustained displacements. (iv) They operate even when bent or stretched. (v) They offer theoretically predictable performance that is scalable in size and force. (vi) They are polymodal, suited to integration in simple arrays or articulated structures. These actuators share a disadvantage that is common to other electromagnetic actuators, which is that higher forces require proportionally higher currents, with the feasible current limited by heating. As introduced here, these devices mitigate this through the use of thermally conductive polymers that greatly reduced heating. They also have the disadvantage of relatively small displacements, although this can be improved through mechanical design. In a broader context, owing to their attractive properties (including stretchability, speed, ease of driving, and scalability), these

actuators could prove useful in applications benefitting from integration in wearable electronics,^[61] microsurgical robotic instruments,^[64] soft MEMS,^[65] acoustic actuators,^[66] microfluidics,^[67] and autonomous soft robotics.^[14] They are more complex to fabricate than simpler pneumatic soft actuators, but are faster, simpler to drive with microelectronics, and easily adaptable to proportional control over a wide dynamic range. The systems illustrated in Figure 4, for example, may have the right characteristics to operate as a tactile display for human–computer interaction, or, in another embodiment, as a microfluidic pump. These systems have the advantage of being amenable to reconfiguration in a variety of formats.

5. Experimental Section

Fabrication for Soft 3D Helical Coil: The soft 3D helical coil is fabricated using roller coating and stencil printing process with a fine carbon rod (CST, The Composites Store, Inc., CA, USA). Details are shown in Section S1 of the Supporting Information. Ecoflex 0030 (Smooth-On, Inc, Easton, PA, USA) which is mixed at weight ratio of 1:1 (part A:part B) was selected due to its high elongation, short curing time, and ease of molding. EGaIn (Sigma-Aldrich Co. LLC, USA) is used as the conductive component due to its high electrical conductivity and ease of use.

Thermal Composite Fabrication: The highly thermal conductivity composite was developed from liquid metal EGaIn and Ecoflex 0030 elastomer (Smooth-On, Inc, Easton, PA, USA). To obtain this solution, liquid Ecoflex 0030 (mixing part A with part B at weight ratio of 1:1) is mixed with EGaIn alloy (Sigma-Aldrich Co. LLC., USA) at a desired weight ratio using a Planetary Centrifugal Mixer (Model Thinky, ARE-310, USA) for 5 min. The thermal composite is subsequently used to fabricate the 3D helical coils where similar steps in previous parts are repeated.

Fabrication Process for the SVAs: The soft VAs, comprised of flexible membranes, 3D helical coils, magnetic shield covers, and silicone substrates, were fabricated using combined techniques of soft lithography, 3D printing, and laser cutting. The permanent magnet was NdFeB, N52 grade from K&J Magnetics, USA. Ecoflex 0030 (Smooth-On, Inc, Easton, PA, USA), which is mixed at a weight ratio of 1:1 (part A:part B) was selected for the soft components due to its high elongation at break. This silicone was mixed with fine iron powder particle (>97.7%, 325 Mesh, ChemicalStore, Inc., USA) with a volume ratio of 3:2 to make the magnetic shield cover. Further details are given in Section S2 of the Supporting Information.

Fabrication Process for Miniature SEMG: The gripper was fabricated using the micromolding process detailed in Section S3 of the Supporting Information. Liquid silicone (Sylgard 184 Silicone Elastomer, Dow Corning, USA) was chosen for the soft magnet due to its ease of molding and slow curing time. The silicone was mixed with magnetic powders, poured onto the printed mold, and aligned under the influence of an external magnetic field. The magnetic powders ($\approx 5 \mu\text{m}$ diameter) were obtained by crushing NdFeB permanent magnet, (N52 grade, K&J Magnetics, USA), via impact hammer. Ecoflex 0030 (Smooth-On, Inc, Easton, PA, USA), which is mixed at a weight ratio of 1:1 (part A:part B), is used for the bending arms.

Thermal Display and Other Measurements: The thermal characterization is shown in Section S4 of the Supporting Information. Thermal images were recorded via thermal imaging camera (FLIR A35 Series, FLIR Systems, Inc., USA). To measure the magnetic field generated from the 3D helical coil, a magnetic Gauss meter (5180 Handheld Portable Gauss meter, F.W. Bell, USA) was used. To detect the displacement of the flexible membrane and magnetic arm, a laser sensor (Model IL-065, Keyence, USA) was used. For force characterization, a FUTEK load cell LSB200 (FUTEK Advanced Sensor Technology, Inc., USA) connected to a real-time controller (QPIDe Data Acquisition Device, Quanser Inc.,

USA) was used, which decoded the signals. Stretching and bending tests for the coil were carried out using a Mark-10 test stand system (Mark-10 Corporation, USA). A laser Doppler vibrometer (PDV-100, Polytec GmbH, USA) was used to characterize the frequency response of the VA. The response time for the vibrotactile actuator and soft gripper were measured using a laser position sensor (Model IL-065, Keyence, USA). All recorded data were processed in the MATLAB environment (MathWorks, Inc., USA).

Supporting Information

Supporting Information is available from the Wiley Online Library or from the author.

Acknowledgements

The authors acknowledge support from the National Science Foundation (NSF-1628831 and NSF-1623459). Special thanks to Dr. Katja C. Seltmann, Katherine Esau Director, Cheadle Center for Biodiversity & Ecological Restoration (CCBER), UC Santa Barbara for providing the biological samples. Thanks to David Bothman, Microfluidics Lab, California NanoSystems Institute (CNSI), and Trevor Marks, Department of Mechanical Engineering, UC Santa Barbara, for assistance with measurement hardware. Many thanks to Yitian Shao from the RE Touch Lab for helping with LDV measurement and signal processing. Thanks to lab members from the RE Touch Lab and Nguyen Research Group, UC Santa Barbara for helping with equipment and reagent materials.

Conflict of Interest

The authors declare no conflict of interest.

Keywords

gallium indium alloys, high thermal conductivity, miniature grippers, soft electromagnetic actuators, soft polymers, soft tactile actuators

Received: January 10, 2018

Published online: March 5, 2018

- [1] M. M. Hamed, V. E. Campbell, P. Rothemund, F. Güder, D. C. Christodouleas, J.-F. Bloch, G. M. Whitesides, *Adv. Funct. Mater.* **2016**, *26*, 2446.
- [2] B. Mosadegh, P. Polygerinos, C. Keplinger, S. Wennstedt, R. F. Shepherd, U. Gupta, J. Shim, K. Bertoldi, C. J. Walsh, G. M. Whitesides, *Adv. Funct. Mater.* **2014**, *24*, 2163.
- [3] C. Peters, O. Ergeneman, P. D. W. García, M. Müller, S. Pané, B. J. Nelson, C. Hierold, *Adv. Funct. Mater.* **2014**, *24*, 5269.
- [4] R. V. Martinez, C. R. Fish, X. Chen, G. M. Whitesides, *Adv. Funct. Mater.* **2012**, *22*, 1376.
- [5] L. Hines, K. Petersen, G. Z. Lum, M. Sitti, *Adv. Mater.* **2016**, *29*, 1603483.
- [6] C. B. Cooper, K. Arutselvan, Y. Liu, D. Armstrong, Y. Lin, M. R. Khan, J. Genzer, M. D. Dickey, *Adv. Funct. Mater.* **2017**, *27*, 1605630.
- [7] S. Zhu, J.-H. So, R. Mays, S. Desai, W. R. Barnes, B. Pourdeyhimi, M. D. Dickey, *Adv. Funct. Mater.* **2013**, *23*, 2308.
- [8] P. Polygerinos, N. Correll, S. A. Morin, B. Mosadegh, C. D. Onal, K. Petersen, M. Cianchetti, M. T. Tolley, R. F. Shepherd, *Adv. Eng. Mater.* **2017**, *19*, e201700016.
- [9] H. M. Le, T. N. Do, S. J. Phee, *Sens. Actuators, A* **2016**, *247*, 323.

- [10] T. N. Do, Y. Visell, *Sci. Rep.* **2017**, *7*, 1753.
- [11] C. Bartolozzi, L. Natale, F. Nori, G. Metta, *Nat. Mater.* **2016**, *15*, 921.
- [12] B. Li, A. K. Fontecchio, Y. Visell, *Appl. Phys. Lett.* **2016**, *108*, 013502.
- [13] M. Amjadi, K.-U. Kyung, I. Park, M. Sitti, *Adv. Funct. Mater.* **2016**, *26*, 1678.
- [14] D. Rus, M. T. Tolley, *Nature* **2015**, *521*, 467.
- [15] O. M. Wani, H. Zeng, A. Priimagi, *Nat. Commun.* **2017**, *8*, 15546.
- [16] J. Biggs, K. Danielmeier, J. Hitzbleck, J. Krause, T. Kridl, S. Nowak, E. Orselli, X. Quan, D. Schapeler, W. Sutherland, J. Wagner, *Angew. Chem., Int. Ed.* **2013**, *52*, 9409.
- [17] G. Guo-Ying, Z. Jian, Z. Li-Min, Z. Xiangyang, *Bioinspiration Biomimetics* **2017**, *12*, 011003.
- [18] G. Z. Lum, Z. Ye, X. Dong, H. Marvi, O. Erin, W. Hu, M. Sitti, *Proc. Natl. Acad. Sci. USA* **2016**, *113*, E6007.
- [19] Z. Jiachen, D. Eric, *Smart Mater. Struct.* **2016**, *25*, 11LT03.
- [20] T. N. Do, T. E. T. Seah, H. K. Yu, S. J. Phee, *PLoS One* **2016**, *11*, e0148035.
- [21] T. N. Do, K. Y. Ho, S. J. Phee, *Sci. Rep.* **2016**, *6*, 39486.
- [22] E. Diller, M. Sitti, *Adv. Funct. Mater.* **2014**, *24*, 4397.
- [23] M. Sitti, H. Ceylan, W. Hu, J. Giltinan, M. Turan, S. Yim, E. Diller, *Proc. IEEE* **2015**, *103*, 205.
- [24] J. Kim, S. E. Chung, S.-E. Choi, H. Lee, J. Kim, S. Kwon, *Nat. Mater.* **2011**, *10*, 747.
- [25] C. Andrew, K. Jongbaeg, L. Liwei, *J. Micromech. Microeng.* **2007**, *17*, 975.
- [26] A. Nisar, N. Afzulpurkar, B. Mahaisavariya, A. Tuantranont, *Sens. Actuators, B* **2008**, *130*, 917.
- [27] M. P. Nemitz, P. Mihaylov, T. W. Barraclough, D. Ross, A. A. Stokes, *Soft Rob.* **2016**, *3*, 198.
- [28] H. Phung, C. T. Nguyen, T. D. Nguyen, C. Lee, U. Kim, D. Lee, J.-D. Nam, H. Moon, J. C. Koo, H. R. Choi, *Meccanica* **2015**, *50*, 2825.
- [29] M. D. Bartlett, N. Kazem, M. J. Powell-Palm, X. Huang, W. Sun, J. A. Malen, C. Majidi, *Proc. Natl. Acad. Sci. USA* **2017**, *114*, 2143.
- [30] M. D. Dickey, *Adv. Mater.* **2017**, *29*, 1606425.
- [31] N. Kazem, T. Hellebrekers, C. Majidi, *Adv. Mater.* **2017**, *29*, 1605985.
- [32] S.-Y. Tang, V. Sivan, P. Petersen, W. Zhang, P. D. Morrison, K. Kalantar-zadeh, A. Mitchell, K. Khoshmanesh, *Adv. Funct. Mater.* **2014**, *24*, 5851.
- [33] S. W. Jin, J. Park, S. Y. Hong, H. Park, Y. R. Jeong, J. Park, S.-S. Lee, J. S. Ha, *Sci. Rep.* **2015**, *5*, 11695.
- [34] B. Aïssa, M. Nedil, M. A. Habib, E. Haddad, W. Jamroz, D. Therriault, Y. Coulibaly, F. Rosei, *Appl. Phys. Lett.* **2013**, *103*, 063101.
- [35] H. Wu, T. W. Odom, D. T. Chiu, G. M. Whitesides, *J. Am. Chem. Soc.* **2003**, *125*, 554.
- [36] B. Li, Y. Gao, A. Fontecchio, Y. Visell, *Smart Mater. Struct.* **2016**, *25*, 075009.
- [37] B. Li, Y. Shi, H. Hu, A. Fontecchio, Y. Visell, *IEEE Sens. J.* **2016**, *16*, 8908.
- [38] B. Li, Y. Shi, A. K. Fontecchio, Y. Visell, *IEEE Trans. Biomed. Eng.* **2017**, *65*, 687.
- [39] V. Saggiomo, A. H. Velders, *Adv. Sci.* **2015**, *2*, 1500125.
- [40] Y. Zhang, F. Zhang, Z. Yan, Q. Ma, X. Li, Y. Huang, J. A. Rogers, *2017*, *2*, 17019.
- [41] S. I. Park, G. Shin, J. G. McCall, R. Al-Hasani, A. Norris, L. Xia, D. S. Brenner, K. N. Noh, S. Y. Bang, D. L. Bhatti, K.-I. Jang, S.-K. Kang, A. D. Mickle, G. Dussor, T. J. Price, R. W. Gereau, M. R. Bruchas, J. A. Rogers, *Proc. Natl. Acad. Sci. USA* **2016**, *113*, E8169.
- [42] M. A. H. Khondoker, D. Sameoto, *Smart Mater. Struct.* **2016**, *25*, 093001.
- [43] I. D. Joshipura, H. R. Ayers, C. Majidi, M. D. Dickey, *J. Mater. Chem. C* **2015**, *3*, 3834.
- [44] N. Lazarus, C. D. Meyer, S. S. Bedair, H. Nochetto, I. M. Kierzewski, *Smart Mater. Struct.* **2014**, *23*, 085036.
- [45] B. J. Carey, J. Z. Ou, R. M. Clark, K. J. Berean, A. Zavabeti, A. S. R. Chesman, S. P. Russo, D. W. M. Lau, Z.-Q. Xu, Q. Bao, O. Kavehei, B. C. Gibson, M. D. Dickey, R. B. Kaner, T. Daeneke, K. Kalantar-Zadeh, *Nat. Commun.* **2017**, *8*, 14482.
- [46] W. Zhang, B. S. Naidu, J. Z. Ou, A. P. O'Mullane, A. F. Chrimes, B. J. Carey, Y. Wang, S.-Y. Tang, V. Sivan, A. Mitchell, S. K. Bhargava, K. Kalantar-zadeh, *ACS Appl. Mater. Interfaces* **2015**, *7*, 1943.
- [47] W. Zhang, J. Z. Ou, S. Y. Tang, V. Sivan, D. D. Yao, K. Latham, K. Khoshmanesh, A. Mitchell, A. P. O'Mullane, K. Kalantar-zadeh, *Adv. Funct. Mater.* **2014**, *24*, 3799.
- [48] V. Sivan, S. Y. Tang, A. P. O'Mullane, P. Petersen, N. Eshtiaghi, K. Kalantar-zadeh, A. Mitchell, *Adv. Funct. Mater.* **2013**, *23*, 144.
- [49] W. Zhang, N. Srivannan, A. F. Chrimes, M. Taylor, K. J. Berean, J. Z. Ou, T. Daeneke, A. P. O'Mullane, G. Bryant, K. Kalantar-zadeh, *Sens. Actuators, B* **2016**, *223*, 52.
- [50] F. Carle, K. Bai, J. Casara, K. Vanderlick, E. Brown, *Phys. Rev. Fluids* **2017**, *2*, 013301.
- [51] I. Alves de Castro, A. F. Chrimes, A. Zavabeti, K. J. Berean, B. J. Carey, J. Zhuang, Y. Du, S. Dou, K. Suzuki, R. Shanks, *Nano Lett.* **2017**, *17*, 7831.
- [52] S. H. Jeong, S. Chen, J. Huo, E. K. Gamstedt, J. Liu, S.-L. Zhang, Z.-B. Zhang, K. Hjort, Z. Wu, *Sci. Rep.* **2015**, *5*, 18257.
- [53] Q. Mu, S. Feng, G. Diao, *Polym. Compos.* **2007**, *28*, 125.
- [54] S. H. Jeong, F. J. Cruz, S. Chen, L. Gravier, J. Liu, Z. Wu, K. Hjort, S.-L. Zhang, Z.-B. Zhang, *ACS Appl. Mater. Interfaces* **2017**, *9*, 15791.
- [55] D. W. Hahn, M. N. Özisik, *Heat Conduction*, Wiley, Hoboken, NJ, USA **2012**.
- [56] K. Bark, E. Hyman, F. Tan, E. Cha, S. A. Jax, L. J. Buxbaum, K. J. Kuchenbecker, *IEEE Trans. Neural Syst. Rehabil. Eng.* **2015**, *23*, 51.
- [57] S. Choi, K. J. Kuchenbecker, *Proc. IEEE* **2013**, *101*, 2093.
- [58] H. A. Sonar, J. Paik, *Front. Robot. AI* **2016**, *2*, 00038.
- [59] P. Won-Hyeong, B. Jin Woo, S. Eun-Jae, K. Sang-Youn, *Smart Mater. Struct.* **2016**, *25*, 115020.
- [60] M. Maisto, C. Pacchierotti, F. Chinello, G. Salvietti, A. D. Luca, D. Prattichizzo, *IEEE Trans. Haptics* **2017**, *10*, 511.
- [61] A. Marette, A. Poulin, N. Besse, S. Rosset, D. Briand, H. Shea, *Adv. Mater.* **2017**, *29*, 1700880.
- [62] J. Zarate, H. Shea, *IEEE Trans. Haptics* **2016**, *10*, 106.
- [63] A. C. Ugural, *Stresses in Beams, Plates, and Shells*, 3rd ed., Taylor & Francis, London **2009**.
- [64] J. J. Rassweiler, R. Autorino, J. Klein, A. Mottrie, A. S. Goezen, J.-U. Stolzenburg, K. H. Rha, M. Schurr, J. Kaouk, V. Patel, P. Dasgupta, E. Liatsikos, *BJU Int.* **2017**, *120*, 822.
- [65] B. Mosadegh, A. D. Mazzeo, R. F. Shepherd, S. A. Morin, U. Gupta, I. Z. Sani, D. Lai, S. Takayama, G. M. Whitesides, *Lab Chip* **2014**, *14*, 189.
- [66] K.-Y. Shin, J.-Y. Hong, J. Jang, *Chem. Commun.* **2011**, *47*, 8527.
- [67] J. Zhang, S. Yan, D. Yuan, G. Alici, N.-T. Nguyen, M. Ebrahimi Warkiani, W. Li, *Lab Chip* **2016**, *16*, 10.

Copyright WILEY-VCH Verlag GmbH & Co. KGaA, 69469 Weinheim, Germany, 2018.



Supporting Information

for *Adv. Funct. Mater.*, DOI: 10.1002/adfm.201800244

Miniature Soft Electromagnetic Actuators for Robotic Applications

*Thanh Nho Do, Hung Phan, Thuc-Quyen Nguyen, and Yon Visell**

Copyright WILEY-VCH Verlag GmbH & Co. KGaA, 69469 Weinheim, Germany, 2018.

Supporting Information

Miniature Soft Electromagnetic Actuators for Robotic Applications

Thanh Nho Do, Hung Phan, Thuc-Quyen Nguyen, and Yon Visell

Dr. Thanh Nho Do and Prof. Yon Visell

Department of Electrical Computer Engineering, Media Arts and Technology Program,
California NanoSystems Institute, University of California, Santa Barbara, CA 93106

E-mails: dothanhnho@ucsb.edu and yonvisell@ece.ucsb.edu

Dr. Hung Phan and Prof. Thuc-Quyen Nguyen

Department of Chemistry and Biochemistry, University of California Santa Barbara, CA 93106
Emails: hphan@chem.ucsb.edu and quyen@chem.ucsb.edu

S1. Fabrication process for the soft 3D helical coil

First, liquid Ecoflex-0030 (Smooth-On, Inc, Easton, PA, USA) is prepared by mixing part A and part B with a weight ratio of 1:1. The mixing process is carried out in a planetary centrifugal mixer (Model Thinky ARE-310, USA) for one minute. Next, the liquid silicone solution is spread onto a glass surface using customized film applicator. The height of the cast silicone layer is controlled to approximately 150 μm by a precision ball screw. A fine carbon fiber rod with a diameter of 200 μm (CST, The Composites Store, Inc., CA, USA) is mounted onto a DC motor (Maxon motor, model DC-MAX26S EB KL 24V, USA) via micro pin vice (162A, L.S. Starrett Company, USA), which subsequently is used to roll the carbon fiber rod onto the laminated silicone layer. The rod and laminated layer are immediately heated using a hotplate (Model HP88854100, The Lab Depot, Inc., USA) at 150 $^{\circ}\text{C}$ for a few seconds to cure the silicone layer. Next, a hollow tube is obtained by directly peeling off the Ecoflex layer from the fiber carbon rod. After that, eutectic gallium indium alloy (EGaIn, Sigma-Aldrich Co. LLC., USA) is injected into the hollow tube via micro needle and syringe. Electric cables are inserted into the two ends of the soft channel for the power supply connection. The resulting soft conductive filament is wrapped around a plastic cylinder with desired inner diameter, turns, and height to form a 3D helical structure. To maintain the 3D shape, a few drops of uncured liquid Ecoflex are applied to the coil, and after 10 minutes are heated at 60 $^{\circ}\text{C}$ for 30 minutes to cure the silicone.

S2. Fabrication process for the soft vibrotactile actuators

To create the soft vibrotactile actuator using the designed soft 3D helical coil, the following processes, which are shown in Figure S2, are used: (i) fabricate a silicone ring to support the flexible membrane, (ii) fabricate the flexible membrane, (iii-iv) fabricate the magnetic shield cover and connected to the permanent magnet. First, a liquid silicone of Ecoflex-0030, Smooth-

On Inc. (Weight ratio 1:1 for Part A:Part B) is deposited onto a silicon wafer via spin coater machine (Model EDC-650-8B from Laurell technologies Corporation, Inc., CA, USA). The obtained layer is then heated in an oven (Model VD 23, BINDER, Germany) for ten minutes at 60⁰C. To obtain a flexible membrane of the desired size and shape, the curing silicon layer is cut using a laser cutting machine (Rayjet 300, Trotec Laser, Inc., MI, USA). A similar process is carried out for the membrane support where a solution between PDMS (Sylgard 184 Silicone Elastomer - Dow Corning, USA) and Ecoflex-0030 (Smooth-On Inc.) with mixing weight ratio (3:7) are used. The mixing solution are deposited onto a 3D printed mold produced via polymer jet deposition printing (Objet 30 Pro, Stratasys Ltd., USA), subsequently cured at 60⁰C for three hours, and cut into desired shape using the Rayjet 300 Laser machine. The permanent magnet is a NdFeB magnet (N52 grade from K&J Magnetics, USA). To cover the magnet with a magnetic shield material, we used a suspension of fine iron powder particle (>97.7%, 325 Mesh, ChemicalStore, Inc., USA) in Ecoflex-0030 with a volume ratio of 3:2. The mixing silicone-powder is obtained using a planetary centrifugal mixer (Model Thinky ARE-310, USA). To make the magnetic shield cover, the mixing solution is poured onto a 3D printed mold and cured it at 70⁰C for two hours. Subsequently, the permanent magnet is inserted into shield cover shell. To obtain the silicone layer as soft subtract for the actuator, the uncured liquid Ecoflex-0030 is laminated onto a flat surface at a desired thickness and cured in an oven at 60⁰C for one hour. All the obtained components are connected together using uncured Ecoflex-0030, Smooth-On Inc. (Weight ratio 1:1 for Part A : Part B) and cured in an oven for one hour.

S3. Fabrication process for miniature soft robotic gripper

First, a permanent cylinder magnet (NdFeB, Grade N52, K&J Magnetics, Inc., USA) is broken down to small magnetic particles using a hammer. The process is repeated for ten to twenty

times to obtain fine micro magnetic particles (approximate diameter 5 μm). Second, a liquid silicone (Sylgard184 Silicone Elastomer - Dow Corning, USA) is homogenously mixed with the magnetic micro particles at a weight ratio of 1:9. The next step is to program the micro magnetic particles in the polymer matrix. The obtained solution is directly poured onto a 3D printed mold and subsequently place above a large permanent magnet (NdFeB, Grade N52, K&J Magnetics, Inc., USA) in a desired orientation. Next, the components are cured in an oven at 60⁰C for three hours. After curing, the aligned soft magnet is manually cut into desired size and shape for soft magnetic arms. To make the soft beam for the magnetic arms, a thin layer of Ecoflex-0030 which is spin-coated onto a silicon wafer and cured at room temperature for two hours is cut into desired shape of the beam using a laser cutting machine. The soft magnet is connected to the soft silicone beam via uncured Ecoflex solution. To make the nail for the arms, a portion of thin yellow Scotch tape (3M, USA) is carefully cut into a triangle shape and attached to the soft magnets by an adhesive glue (Loctite, USA). The flexible beam is obtained from a laser machine with designed shape of silicone thin layer (Ecoflex-0030, Smooth-On, Inc., USA). Once the connectors have fully cured, micro grippers with their attached nails are connected to two soft 3D coils via a liquid Ecoflex-0030 layer.

S4. Thermal characterization

Four different samples of 3D helical coils are fabricated using different thermal composite solutions (weight ratios between liquid metal EGaIn and Ecoflex-0030 are 0%, 30%, 60%, 90%). A thermal camera (FLIR A35 Series, FLIR Systems, Inc., USA) is used to capture the thermal effects on the 3D helical coils. A high current of 2 Amperes from a DC power supply is directly applied to the four helical coils in a period of time ranging from 0 s to 29 s and this current is

removed from the rest of experimental process. Real-time thermal displays are captured for every 6s during the testing.

S5. Magnetic field and magnetic force for the soft 3D coil interacting with the permanent magnet

Consider a flux loop located at distance z' with thickness dz' . The current I passing through the section of this loop (as shown in Figure S1) is given by:

$$dI = I(ndz') = \frac{IN}{l} dz' \quad (\text{S1})$$

where $n = \frac{N}{l}$ is the number of turns per unit length. The magnetic field B_c at distance z from the coil center is:

$$dB_c = \frac{\mu_0 R^2}{2[(z-z')^2+R^2]^{\frac{3}{2}}} dI = \frac{\mu_0 R^2}{2[(z-z')^2+R^2]^{\frac{3}{2}}} \frac{IN}{l} dz' \quad (\text{S2})$$

with R the radius of the coil.

Integrating Equation S2 over the entire length, we obtain an expression for the magnetic field B_c :

$$B_c(z) = \frac{B_0}{2l} \left[\frac{\frac{l}{2}-z}{\sqrt{\left(z-\frac{l}{2}\right)^2+R^2}} + \frac{\frac{l}{2}+z}{\sqrt{\left(z+\frac{l}{2}\right)^2+R^2}} \right] \quad (\text{S3})$$

where $B_0 = \mu_0 NI$ is the nearly uniform magnetic field inside the coil, N is the number of turns, I is the applied current, and $\mu_0 = 4\pi \times 10^{-7} \text{ JA}^{-2}\text{m}^{-1}$ is the magnetic permeability of the core region. ^[1, 2]

The amount of electrical power dissipated via Joule heating can be calculated directly from the electrical resistance of the coil:

$$P_0 = \frac{I^2 \rho l_{\text{conductor}}}{A} \quad (\text{S4})$$

where $\rho, l_{\text{conductor}}, A$ are the electrical conductivity, total length, and cross-sectional area of the conductor. At high powers, heating causes an increase of resistance, which can be accounted for via a thermal factor: [1, 2]

$$P = P_0(1 + \alpha \Delta T) \quad (\text{S5})$$

where ΔT is the increase in coil temperature and α is the linear temperature coefficient of electrical resistivity for the conductive channel.

The magnetic force between a coil and a permanent magnet is given by: [3]

$$F = \int (M_m \cdot \nabla) B_c dV_m \quad (\text{S6})$$

Where F is the force, V_m is the volume of the magnet, M_m is its magnetization and ∇ is the gradient operator defined by $\nabla^T = \left[\frac{\partial}{\partial x} \frac{\partial}{\partial y} \frac{\partial}{\partial z} \right]$

Assuming that the field and gradient components are uniform over the magnet, the force interaction can be written as:

$$F = V_m (M_m \cdot \nabla) B_c \quad (\text{S7})$$

and

$$(M_m \cdot \nabla) = (M_m^T \nabla) = \left[M_x \frac{\partial}{\partial x} M_y \frac{\partial}{\partial y} M_z \frac{\partial}{\partial z} \right] \quad (\text{S8})$$

The permanent magnet is magnetized along the z axis, the above equation can be simplified to:

$$F = M_m V_m \frac{\partial B_c}{\partial z}$$

Or

$$F = M_m V_m \frac{B_0}{2l} \left(\frac{1}{\left(\left(z + \frac{l}{2} \right)^2 + R^2 \right)^{\frac{3}{2}}} - \frac{1}{\left(\left(z - \frac{l}{2} \right)^2 + R^2 \right)^{\frac{3}{2}}} \right) \quad (\text{S9})$$

S6. Membrane deflection

The force-displacement relation may be obtained by considering the effect of a shear force P per unit length, uniformly distributed over the inner radius b , corresponding to net force $F = 2\pi bP$.

The governing equation for a circular plate under axisymmetric loading reads:

$$\nabla^4 \delta(r) = \frac{-Q}{D} \quad (\text{S10})$$

where $\delta(r)$ is the normal displacement, $D = \frac{Eh^3}{12(1-\vartheta^2)}$ is the flexural rigidity of the flexible membrane, E is the elastic modulus, h is thickness of the circular membrane, and ϑ is the Poisson ratio.^[4, 5] Since the load is axisymmetric and the applied radial force is zero, one obtains for the vertical shear response to load Q ^[6]

$$\frac{d}{dr} \left[\frac{1}{r} \frac{d}{dr} \left(r \frac{d\delta}{dr} \right) \right] = \frac{-Q}{D} \quad (\text{S11})$$

If Q is applied at an inner radius b with force P per unit length, then $Q = \frac{-Pb}{r}$. Letting $q = \frac{Pb}{4D}$, one can integrate Equation S11 to obtain

$$\delta(r) = qr^2(\log(r) - 1) + \frac{c_1 r^2}{4} + c_2 \log(r) + c_3 \quad (\text{S12})$$

The solution for $\delta(r)$ is obtained by applying the boundary conditions and solving for the unknown constants c_1 , c_2 , and c_3 .

At the outer edge, $r = a$, one has $\delta(a) = 0$ and $M_r(a) = 0$ where $M_r = -D \left(\frac{d^2\delta}{dr^2} + \frac{\vartheta}{r} \frac{d\delta}{dr} \right)$ is the bending moment.

$$\delta(a) = qa^2(\log(a) - 1) + \frac{c_1 a^2}{4} + c_2 \log(a) + c_3 = 0 \quad (\text{S13})$$

$$M_r(a) = \delta'(a) = q(2a \log(a) - a) + \frac{c_1 a}{2} + \frac{c_2}{a} = 0 \quad (\text{S14})$$

At $r = b$, one has the boundary condition $M_r(b) = 0$

$$M_r(b) = \delta'(b) = q(2b \log(b) - b) + \frac{c_1 b}{2} + \frac{c_2}{b} = 0 \quad (\text{S15})$$

Upon substituting into the general solution given by Equation S12, one obtains

$$\delta(r) = \frac{Pa^2b}{4D} \left(\left(1 - \frac{r^2}{a^2} \right) \left(\frac{2+\vartheta}{2+2\vartheta} - \frac{b^2}{a^2-b^2} \log \frac{b}{a} \right) + \frac{r^2}{a^2} \log \frac{r}{a} + \frac{2b^2}{a^2-b^2} \frac{1+\vartheta}{1-\vartheta} \log \frac{b}{a} \log \frac{r}{a} \right) \quad (\text{S16})$$

The maximum deflection in response to applied force F is given by:

$$\delta_{max} = \frac{Fa^2}{8\pi D} \left(\left(1 - \frac{b^2}{a^2} \right) \left(\frac{2+\vartheta}{2+2\vartheta} - \frac{b^2}{a^2-b^2} \log \frac{b}{a} \right) + \frac{b^2}{a^2} \log \frac{b}{a} + \frac{2b^2}{a^2-b^2} \frac{1+\vartheta}{1-\vartheta} \left(\log \frac{b}{a} \right)^2 \right) \quad (\text{S17})$$

S7. Magnetic torque calculation for miniature gripper

The magnetic particles in each arm experience a torque $T_m = m \times B_c$ due to the applied field B_c generated by the coil, where m is the magnetic moment. The net torque actuated on an arm is given by

$$T_{\text{arm}} = (M \times B_c)V = |M||B_c|V \sin \varphi \quad (\text{S18})$$

where M and $V = t_2 t_4 t_5$ are the magnetization and volume of the soft magnet, and $\varphi = \frac{\pi}{2} - \alpha - \gamma$ where α is the relative magnet polarization (Figure 6E) and γ is the bending angle of the

flexible arm joint, a beam of cast polymer (Ecoflex-0030). Accounting for the joint stiffness, in equilibrium, for small deformations, one has

$$T_{\text{arm}} = EI_b \frac{\gamma}{t_3} \quad (\text{S19})$$

where E , $I_b = \frac{t_1 t_6^3}{12}$, γ , and t_3 are Young modulus, second moment of area, bending angle, and length of polymer beam, respectively. t_1, t_6 are the width and height of the polymer beam cross section (See Figure 6).

The applied magnetic field B_c and bending angle γ are related by

$$B_c(\gamma) = \frac{\gamma EI_b}{|M|t_2 t_3 t_4 t_5 \cos(\alpha + \gamma)} \quad (\text{S20})$$

S8. Magnetic field calculation for the soft permanent magnet

The magnetic field B_m at a distance y from a cylinder magnet with length D_m , radius R_m (Figure S3) is given by:

$$B_m(y) = \frac{B_r}{2} \left[\frac{D_m + y}{\sqrt{(D_m + y)^2 + R_m^2}} - \frac{y}{\sqrt{y^2 + R_m^2}} \right] \quad (\text{S21})$$

where B_r is the remanence field and independent of the magnet geometry, y is the distance from the pole face on the symmetrical axis, D_m is thickness (height) of the cylinder magnet, and R_m is the radius of the magnet.

We measure the magnetic field to the surface ($y = 0$) of a permanent, elastic magnet (the fabrication was carried out at a predetermined ratio 1:9 of PDMS and magnetic powder. The ratio of reagents in the PDMS mixture was 1:10 (ratio of curing agent to elastomer)). The

diameter for the magnet is as follow: $D_m = 4.4 \text{ mm}$, $R_m = 3.15 \text{ mm}$. The magnetic field obtained at the surface is 0.07T . Using the above equation, we can obtain $B_r = 0.172\text{T}$

The magnetization M of this magnet can be calculated using:

$$M = \frac{B_r}{\mu_0} = \frac{0.172}{4\pi \times 10^{-7}} = 137 \text{ kAm}^{-1} \quad (\text{S22})$$

Where $\mu_0 = 4\pi \times 10^{-7} \text{ JA}^{-2}\text{m}^{-1}$ is the magnetic vacuum permeability.

S9. Numerical identification of the relation between magnetic field and bending angle

The nonlinear relation between magnetic field and the bending angle of the gripper arm not admit any simple analytical solution for the angle. To compare with experimental measurements, we used a simple numerical solution technique based on Newton's method.

Recalling the relation between applied magnetic field and bending angle from Equation S20, we have:

$$B_c(\gamma) = \frac{\gamma EI_b}{|M|t_2 t_3 t_4 t_5 \cos(\alpha + \gamma)} \quad (\text{S23})$$

or

$$\frac{\cos(\alpha + \gamma)}{\gamma} = \frac{EI_b}{|M|t_2 t_3 t_4 t_5 B_c(\gamma)} \quad (\text{S24})$$

Define a function $f(\gamma) = \frac{EI_b}{|M|t_2 t_3 t_4 t_5 B_c(\gamma)} \gamma - \cos(\alpha + \gamma)$. The derivative of this function is:

$$f'(\gamma) = \frac{EI_b}{|M|t_2 t_3 t_4 t_5 B_c(\gamma)} + \sin(\alpha + \gamma) \geq 0 \quad (\text{S25})$$

This implies that, within a suitable domain, the function $f(\gamma)$ always has a unique solution for γ .

Note that $(\alpha + \gamma) \leq 180^\circ$, then $\sin(\alpha + \gamma) \geq 0$

Applying Newton's method with a starting guess γ_0 , one can obtain the solution of γ from Equation S25:

$$\gamma_{n+1} = \gamma_n - \frac{f(\gamma_n)}{f'(\gamma_n)} \quad (\text{S26})$$

With parameters $M = 137 \text{ kAm}^{-1}$, $t_1 = 0.9 \text{ mm}$, $t_2 = 1 \text{ mm}$, $t_3 = 0.6 \text{ mm}$, $t_4 = 1.9 \text{ mm}$, $t_5 = 0.7 \text{ mm}$, $t_6 = 0.23 \text{ mm}$, $E = 125 \text{ kPa}$, $\alpha = 25^0 \times 180/\pi$. For all cases, the values of γ converge with $n=10$, $\gamma_0 = 0$.

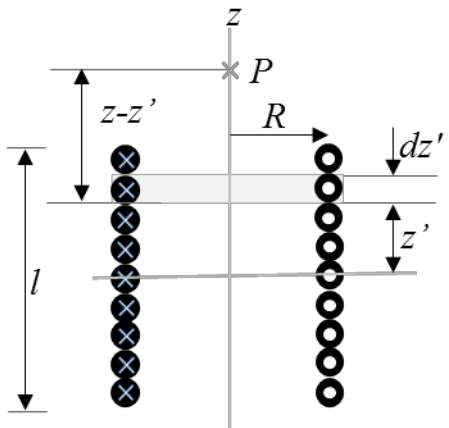


Figure S1. Cross-sectional view of a finite solenoid with length l , inner radius R , and number of turns N .

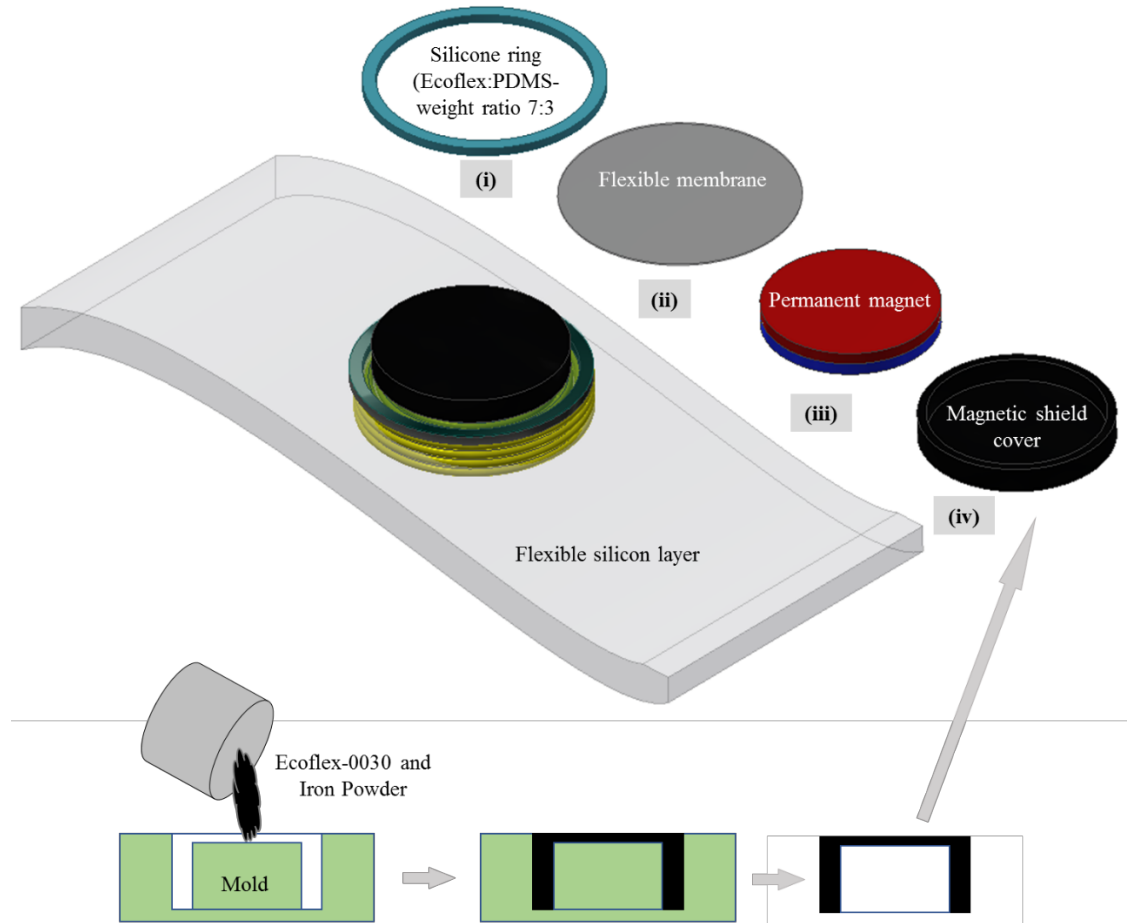


Figure S2. Fabrication process for a soft vibrotactile actuator and the magnetic shield cover. Note that the cover is used to minimize interaction forces between electromagnets in an array.

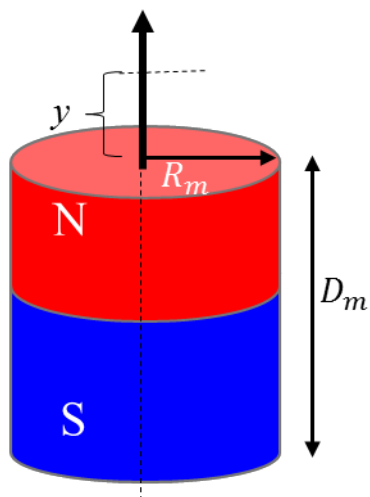


Figure S3. The magnetic field B_m at a distance y from a cylinder magnet with length D_m and radius R_m

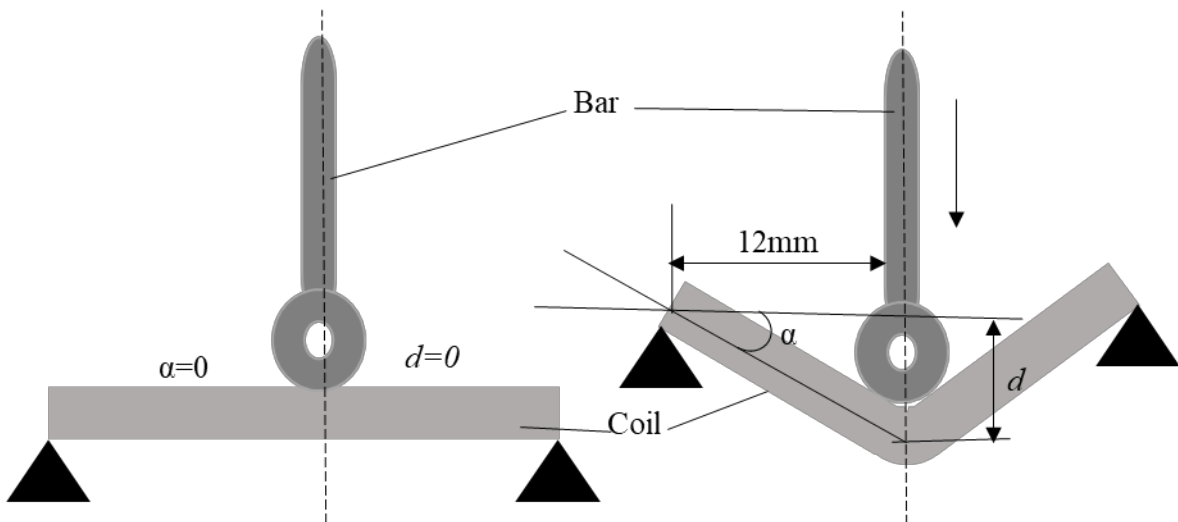


Figure S4. Bending angle calculation for the coil ($\alpha = \tan^{-1}(d/12)$) where d is vertical displacement obtained from laser sensor. The coil is fixed onto a frame. A bar mounted onto a linear slider (Mark-10 test stand system, Mark-10 Corporation, USA) is gradually moved from the top to the bottom (travel distance d) to provide the bending angle for the soft coil.

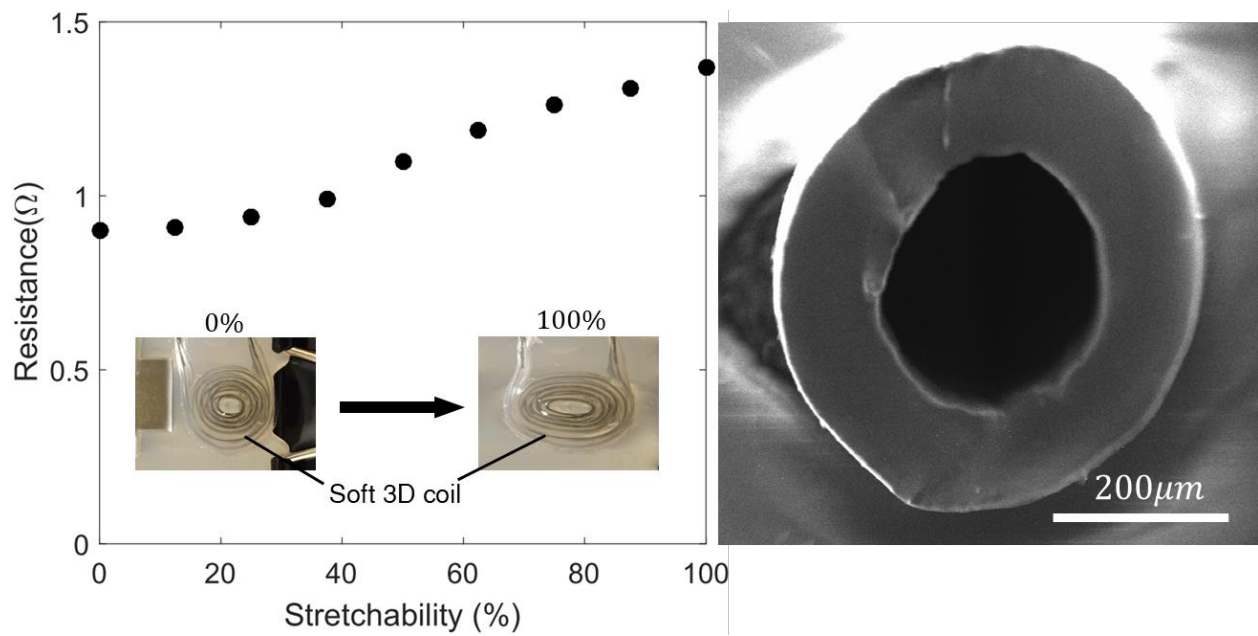


Figure S5. Resistance characterization for the soft 3D coil. (Left panel) Resistance versus stretchability, (Right panel). Cross-sectional SEM image for the cross section of the hollow filament.

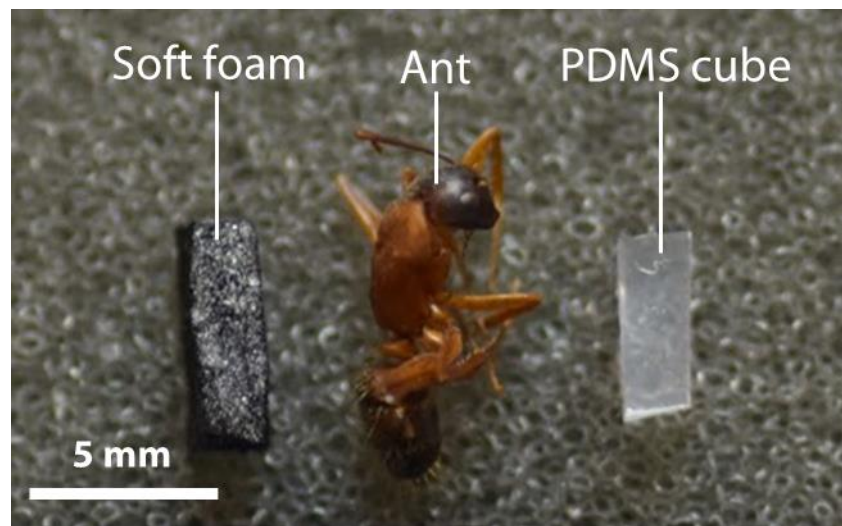


Figure S6. Experimental objects for soft magnetic gripper. (From left to right): Soft foam (weight 2.89 mg), an ant (weight: 3.61 mg), and PDMS cube (weight: 13 mg). Scale bar: 5mm

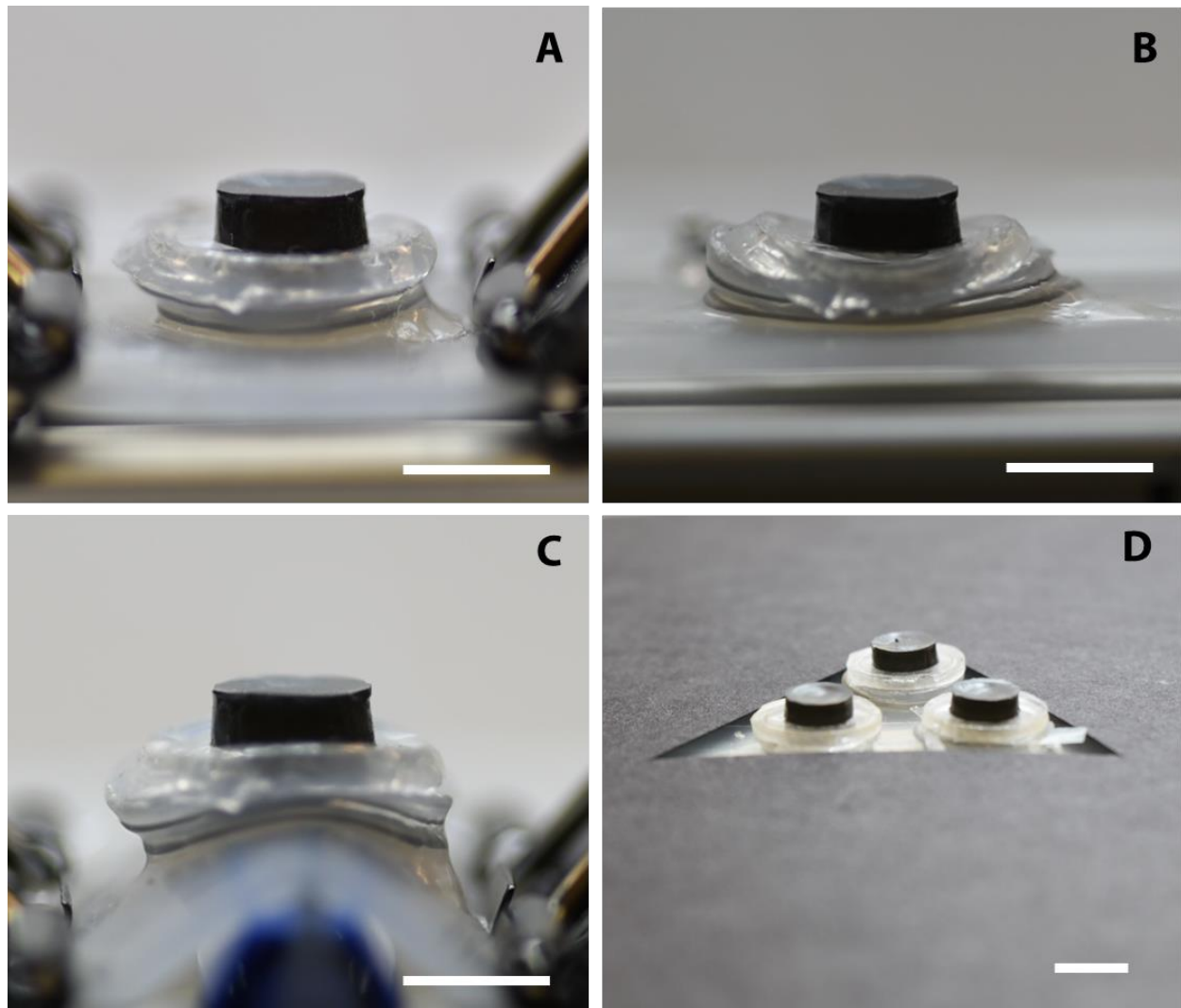


Figure S7: Characterization for soft electromagnetic vibrotactile actuators. A) Non-stretchable configuration. B) Under 75% of strain C) Under bending. D) Array of soft vibrotactile actuators.

Scale bar: 5 mm

Table S1. Comparison between proposed soft actuators with other available actuators

	Work density (kJm^{-3})	Bandwidth (Hz)	Driving voltage
Dielectric elastomers ^[7, 8]	10 typical	1400 at -3 dB, maximum observed $> 50 \text{ kHz}$ (requires costly driving electronics)	$> 1 \text{ kV}$
Pneumatic actuator ^[9-11]	100–200	1–10	1 – 10 V (for valve control)
Ionic Polymer Metal Composites (IPMC) ^[9, 12]	5.5	< 1	5–7 V
Soft vibrotactile actuator presented here	0.0053	> 500	0.5–1 V
Soft magnetic gripper presented here	0.25×10^{-3}	> 45	0.5–1 V
Carbon nanotube actuator ^[7]	2 typical, 40 max	<1	2 V

References

- [1] J. D. Jackson, *Classical Electrodynamics Third Edition*, Wiley, 1998.
- [2] J. J. Zárate, G. Tosolini, S. Petroni, M. De Vittorio, H. Shea, Sensors and Actuators A: Physical 2015, 234, 57.
- [3] N. J. Groom, NASA TM-100671 Septemper 1988.
- [4] P. Yong-Lae, M. Carmel, K. Rebecca, B. Phillippe, J. W. Robert, Journal of Micromechanics and Microengineering 2010, 20, 125029.
- [5] Y. Huang, Y. Wang, L. Xiao, H. Liu, W. Dong, Z. Yin, Lab on a Chip 2014, 14, 4205.
- [6] A. C. Ugural, *Stresses in Beams, Plates, and Shells, Third Edition*, Taylor & Francis, 2009.
- [7] J. D. W. Madden, N. A. Vandesteeg, P. A. Anquetil, P. G. A. Madden, A. Takshi, R. Z. Pytel, S. R. Lafontaine, P. A. Wieringa, I. W. Hunter, IEEE Journal of Oceanic Engineering 2004, 29, 706.
- [8] G. Guo-Ying, Z. Jian, Z. Li-Min, Z. Xiangyang, Bioinspiration & Biomimetics 2017, 12, 011003.
- [9] M. Shahinpoor, K. J. Kim, Smart materials and structures 2001, 10, 819.
- [10] M. Wehner, M. T. Tolley, Y. Mengüç, Y.-L. Park, A. Mozeika, Y. Ding, C. Onal, R. F. Shepherd, G. M. Whitesides, R. J. Wood, Soft Robotics 2014, 1, 263.
- [11] R. Versluys, K. Deckers, M. Van Damme, R. Van Ham, G. Steenackers, P. Guillaume, D. Lefeber, Applied Bionics and Biomechanics 2009, 6, 3.
- [12] M. Shahinpoor, Y. Bar-Cohen, J. Simpson, J. Smith, Smart materials and structures 1998, 7, R15.

List of Supporting videos

Video 1. Soft vibrotactile actuator at 5 Hz

Video 2. Soft vibrotactile actuator at 10 Hz

Video 3. Soft vibrotactile actuator at 20 Hz

Video 4. Soft vibrotactile actuator at 40 Hz

Video 5. Soft vibrotactile actuator being bent

Video 6. Soft vibrotactile actuator being stretched

Video 7. Soft vibrotactile actuator with tactile display

Video 8. Micro gripper at 1 Hz

Video 9. Micro gripper at 5 Hz

Video 10. Micro gripper at 15 Hz

Video 11. Micro gripper at 25 Hz

Video 12. Micro gripper at 45 Hz

Video 13. Micro gripper with foam

Video 14. Micro gripper with ant

Video 15. Micro gripper with PDMS